European Journal of Medicinal Chemistry 227 (2022) 113915

Contents lists available at ScienceDirect

European Journal of Medicinal Chemistry

journal homepage: http://www.elsevier.com/locate/ejmech

Pyridazino-pyrrolo-quinoxalinium salts as highly potent and selective leishmanicidal agents targeting trypanothione reductase

Héctor de Lucio [a4, **], Javier García-Marín [b, c, d, 1, 4], Patricia Sánchez-Alonso [b, 2], Juan Carlos García-Soriano [a], Miguel Ángel Toro [a, 3], Juan J. Vaquero [b, c, d], Federico Gago [e], Ramón Alajarín [b, c, d], Antonio Jiménez-Ruiz [a, *]

[a] Departamento de Biología de Sistemas, Universidad de Alcalá, E-28805, Alcalá de Henares, Madrid, Spain
[b] Departamento de Química Orgánica y Química Inorgánica, Universidad de Alcalá, 28805, Alcalá de Henares, Madrid, Spain
[c] Instituto Ramón y Cajal de Investigación Sanitaria (IRYCIS) Ctra, Colmenar Viejo, km. 9100, 28034, Madrid, Spain
[d] Instituto de Investigación Química Andrés Manuel del Río (IQAR), Universidad de Alcalá, 28805, Alcalá de Henares, Madrid, Spain
[e] Área de Farmacología, Departamento de Ciencias Biomédicas, Unidad Asociada al IQM-CSIC, Universidad de Alcalá, E-28805, Alcalá de Henares, Madrid, Spain

ARTICLE INFO

Article history:
Received 30 July 2021
Received in revised form
7 October 2021
Accepted 8 October 2021
Available online 15 October 2021

Keywords:
Pyridazino[2,3-*a*]pyrrolo[2,1-*c*]quinoxalinium
Leishmania
Trypanothione disulfide reductase
Enzyme inhibitor

ABSTRACT

Fifteen pyridazino-pyrrolo-quinoxalinium salts were synthesized and tested for their antiprotozoal activity against *Leishmania infantum* amastigotes. Eleven of them turned out to be leishmanicidal, with EC_{50} values in the nanomolar range, and displayed low toxicity against the human THP-1 cell line. Selectivity indices for these compounds range from 10 to more than 1000. Compounds **3b** and **3f** behave as potent inhibitors of the oxidoreductase activity of the essential enzyme trypanothione disulfide reductase (TryR). Interestingly, binding of **3f** is not affected by high trypanothione concentrations, as revealed by the noncompetitive pattern of inhibition observed when tested in the presence of increasing concentrations of this substrate. Furthermore, when analyzed at varying NADPH concentrations, the characteristic pattern of hyperbolic uncompetitive inhibition supports the view that binding of NADPH to TryR is a prerequisite for inhibitor-protein association. Similar to other TryR uncompetitive inhibitors for NADPH, **3f** is responsible for TryR-dependent reduction of cytochrome *c* in a reaction that is typically inhibited by superoxide dismutase.

1. Introduction

Parasites of the genus *Leishmania* are the causative agents of leishmaniasis, a neglected tropical disease transmitted by dipterous insects from the Psychodidae family. It is endemic in 98 countries and approximately 15 million of new cases are diagnosed every year, leading to high rates of morbidity and mortality. The most lethal form of the disease is visceral leishmaniasis (VL –also known as kala-azar–), predominantly caused by *Leishmania donovani* and *Leishmania infantum* species, which inevitably leads to death if left untreated [1]. Unfortunately, despite being one of the major neglected tropical diseases in terms of number of cases and death rate, there is still no effective vaccine for leishmaniasis. Furthermore, none of the drugs currently in use can be considered ideal due to their high toxicity, numerous side effects and the need for long treatments. The sum of these caveats leads to frequent therapeutic noncompliance [2,3].

The pyrroloquinoxaline heterocyclic framework makes up the basis of an important class of compounds possessing interesting biological activities. Derivatives of this tricyclic system have been studied as ligands of pharmacological membrane receptors [4], inhibitors of protein kinases [5] and phosphatases [6], and also as

* Corresponding author.
** Corresponding author.
E-mail addresses: hector.lucio@edu.uah.es (H. de Lucio), javier.garciamarin@uah.es (J. García-Marín), sanchezalonsopatricia@gmail.com (P. Sánchez-Alonso), jcarlos.garcias@uah.es (J.C. García-Soriano), migueltoro83@gmail.com (M.Á. Toro), juanjose.vaquero@uah.es (J.J. Vaquero), federico.gago@uah.es (F. Gago), ramon.alajarin@uah.es (R. Alajarín), antonio.jimenez@uah.es (A. Jiménez-Ruiz).
[1] Current address J. G.-M., Chemical and Physical Biology Department, Centro de Investigaciones Biológicas, CIB–CSIC, C/Ramiro de Maeztu, 9, 28040, Madrid, Spain.
[2] Current address P. S.-A., Alfa Bioresearch Co., Madrid, Spain.
[3] Current address M. A. T., Centro Nacional de Secuenciación Genómica-CNSG, Universidad de Antioquia, Medellín, Antioquia, Colombia.
[4] These two authors contributed equally to this work.

https://doi.org/10.1016/j.ejmech.2021.113915

antifungal [7] and antiparasitic (antimalarial, antileishmanial) agents [8–12]. 4-Substituted pyrrolo[1,2-*a*]quinoxaline derivatives were designed and tested against *Leishmania amazonensis* and *Leishmania infantum* promastigotes [8].

Because of our previous experience in the synthesis of protein tyrosine phosphatase 1B (PTP1B) inhibitors containing a pyrroloquinoxaline scaffold [6,13,14], we started a program based on this chemotype for the design of new molecules possibly endowed with leishmanicidal activity. Initially we found the pyridazino[2,3-*a*]pyrrolo[2,1-c]quinoxal-13-inium scaffold as a hit and then we carried out the synthesis of a library of 15 compounds that were tested against axenic and intracellular *L. infantum* amastigotes. The most active molecules were also tested for their inhibitory activity against *L. infantum* trypanothione disulfide reductase (*Li*TryR), one of the most widely studied targets in these parasites. This enzyme catalyzes electron transfer from NADPH to oxidized trypanothione (TS_2) to yield reduced trypanothione ($T(SH)_2$), a thiol-containing molecule essential for redox homeostasis in all trypanosomatids.

Herein we report the synthesis and structure-activity relationship (SAR) studies of novel pyridazino-pyrrolo-quinoxalinium salts of general formulae 3 (Scheme 1) and demonstrate the potential of this novel chemotype for *Li*TryR inhibition and leishmanicidal activity against *L. infantum* parasites. A whole set of 15 pyridazino-pyrrolo-quinoxalinium-based compounds modified at four different positions in a new scaffold was prepared and evaluated. Eleven of these molecules display submicromolar activity against axenic amastigotes and two of them show EC_{50} values of 1–2 μM in intracellular infection assays. This potent leishmanicidal activity is associated with very low toxicity against human THP-1 cells, thus giving rise to very good selectivity indices that, for two compounds, are greater than 300. Compound **3f**, selected as the most active molecule against the intracellular parasites, behaves as a noncompetitive hyperbolic inhibitor of *Li*TryR when tested against increasing concentrations of TS_2 as substrate and as an uncompetitive hyperbolic inhibitor when assayed against increasing concentrations of NADPH.

2. Results and discussion

2.1. Chemistry

4-Substituted pyrrolo[1,2-*a*]quinoxaline derivatives have previously been reported as active against *Leishmania amazonensis* and *Leishmania infantum* promastigotes [8,11]. Our former experience in the synthesis of enzyme inhibitors containing a pyrroloquinoxaline scaffold [6,13,14] drove us to conduct a preliminary screening of pyrroloquinoxalines against *L. infantum* axenic amastigotes. Pyrroloquinoxalines **1** were prepared by classical synthesis using commercially available 2-nitroanilines, thus limiting the possible combinations of R_1 and R_2 substituents to the pyrroloquinoxaline derivatives **1a-i** (Scheme 1) [6]. The synthetic procedure involves four steps: acetylation of *o*-nitroanilines; reduction of the nitro group to amine; Clauson-Kaas pyrrole synthesis; and finally cyclization using $POCl_3$. However, the assayed compounds **1** showed low activity against *Leishmania* axenic amastigotes (see next section, *Biological evaluation*). In view of these results and considering our former experience on cationic polycyclic heterocycles as cytotoxic and DNA-intercalator compounds [15,16], for the next round of modifications, we decided to introduce a new heterocyclic ring with a quaternary nitrogen atom, the pyridazinium ring. Thus, once prepared, compounds of series **1** were treated with *O*-(mesitylenesulfonyl)hydroxylamine (MSH, CAUTION! This reagent may produce explosions if excess of perchloric acid is not thoroughly washed out with plenty of water) to give *N*-aminoquinoxalinium salt **2** intermediates in medium to high yield (see Supporting Information). Thereafter, a Westphal condensation reaction was performed between series **2** intermediates and a symmetrical 1,2-diketone in the presence of a base. The best conditions were explored for each diketone and five methods were set up to give pyridazino-pyrrolo-quinoxalinium salts **3** in moderate to high yield (Table 1). Unexpectedly, during the reactions of **2b** and **2c** with hexane-3,4-dione under Westphal conditions, the ylides **4b** and **4c** were obtained. These ylides were then treated with hydrobromic acid to provide pyridazino-pyrrolo-quinoxalinium salts **3e** and **3f**, respectively (Table 1). All in all, we carried out the synthesis of a library of 15 new compounds containing the pyridazino[2,3-*a*]

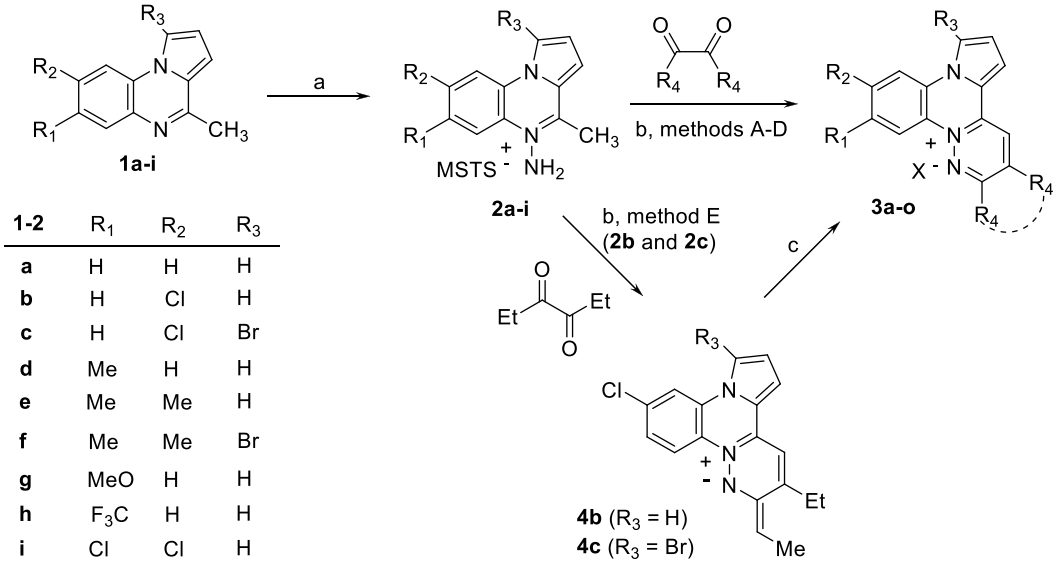

1-2	R_1	R_2	R_3
a	H	H	H
b	H	Cl	H
c	H	Cl	Br
d	Me	H	H
e	Me	Me	H
f	Me	Me	Br
g	MeO	H	H
h	F_3C	H	H
i	Cl	Cl	H

Scheme 1. Synthesis of pyridazino-pyrrolo-quinoxalinium salts **3**. *Conditions:* a. MSH [(mesitylenesulfonyl)hydroxylamine], CH_2Cl_2; b. Methods (1,2-diketone, base, solvent, temp): A (butane-2,3-dione, Et_3N, ethanol, r.t.); B (dioxane-2,3-diol, Et_3N, ethanol, reflux); C (acenaphthoquinone, AcONa, acetone, reflux); D (hexane-3,4-dione, Et_3N, methanol, reflux); E (hexane-3,4-dione −2 equiv-, Et_3N, methanol, reflux); c. 46% HBr.

Table 1
Synthesized compounds **3** and yields obtained. Structure for **3b** (*4H*-acenaphtho[*1′,2′:3,4*]pyridazino[2,3-*a*]pyrrolo[2,1-*c*]quinoxal-9-inium) is also drawn.

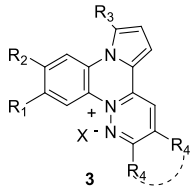

3

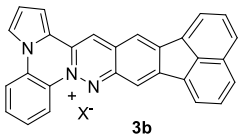

3b

3	R_1	R_2	R_3	R_4	Yield (%)	Method[a]
a	H	H	H	Me	34	A
b	H	H	H	acenaphtho-1,8-diyl	62	C
c	H	Cl	H	H	47	B
d	H	Cl	H	Me	42	A
e	H	Cl	H	Et	41	E
f	H	Cl	Br	Et	97	E
g	Me	H	H	Me	46	A
h	Me	Me	H	H	58	B
i	Me	Me	H	Me	56	A
j	Me	Me	H	Et	68	D
k	Me	Me	Br	H	59	B
l	Me	Me	Br	Me	91	A
m	MeO	H	H	Me	38	A
n	F_3C	H	H	Me	48	B
o	Cl	Cl	H	Me	35	A

[a] Conditions and procedures are detailed in Scheme 1 and Experimental Section. For compounds **3**, X^- is mesitylenesulfonate ($MSTS^-$) except for **3e** and **3f**, where X^- is bromide.

pyrrolo[2,1-c]quinoxal-13-inium scaffold for testing against *Leishmania* parasites.

2.2. Biological evaluation

A subset of pyrroloquinoxalines **1** (**1a**, **1b** and **1f**) were tested for their ability to kill *Leishmania infantum* axenic amastigotes. The results obtained in this preliminary screening revealed a low leishmanicidal activity of these compounds. In fact, the EC_{50} values obtained for the three pyrroloquinoxalines assayed are well above 25 μM.

To improve the antileishmanial activity of these derivatives, a novel pyridazino[2,3-*a*]pyrrolo[2,1-c]quinoxal-13-inium scaffold was designed by introducing a pyridazinium ring with a quaternary nitrogen atom. Then, the 15 pyridazino-pyrrolo-quinoxalinium salts (**3a-o**) were tested for their antiprotozoal activity against *L. infantum* axenic amastigotes using miltefosine as the reference drug. Cytotoxicity was assayed on the human monocytic cell line THP-1. According to the results shown in Table 2, the EC_{50} values obtained for eleven of these compounds against axenic amastigotes are in the nanomolar range. Indeed, compounds **3b**, **3c**, **3e**, **3f** and **3j** show EC_{50} values below 100 nM. In spite of these promising results, we could only establish weak structure-activity relationships. Notably, with the exception of **3j**, all the compounds bearing any substituent at R_1 show higher EC_{50} values against *L. infantum* axenic amastigotes ranging from 0.3 to 3.8 μM. We also observed that, with the exception of **3d** and **3o** with a methyl group in R_4, all the compounds bearing a chloro atom in R_2 (**3c**, **3e** and **3f**) show a potent and selective antileishmanial activity. Regarding the R_4 substituent, the presence of an ethyl group in compounds **3e**, **3f** and **3j** is another common feature of three of the best leishmanicidal agents. Interestingly, the octacyclic 9-inium cation **3b**, which was synthesized to explore the effect of having more than one ring condensed to the intermediate salt **2a**, exhibits a potent leishmanicidal and cytotoxic activity.

On the other hand, LC_{50} values on THP-1 cells are in most cases over 10 μM. This low toxicity, together with their excellent activity against axenic amastigotes, gives rise to selectivity indices (SI) > 20 for 10 compounds and >300 for two of them (**3c** and **3e**). Compared to previously reported 4-substituted pyrrolo[1,2-*a*]quinoxaline derivatives [8], the EC_{50} values obtained for most of the pyridazino-pyrrolo-quinoxalinium salts against the parasites are 10-fold lower and, importantly, their SI values are increased up to a hundred times.

Table 2
Leishmanicidal and cytotoxic activity for pyridazino-pyrrolo-quinoxalinium salts **3** on *L. infantum* axenic amastigotes and THP-1 monocytes, respectively.

Compound	EC_{50} (μM) Amastigotes[a]	LC_{50} (μM) THP-1[b]	SI[c]
3a	0.90 ± 0.24	>25	>27.78
3b	0.04 ± 0.00	1.02 ± 0.04	25.5
3c	0.02 ± 0.01	20.23 ± 1.59	1011.5
3d	0.24 ± 0.04	15.56 ± 0.29	64.8
3e	0.08 ± 0.01	24.32 ± 2.16	304
3f	0.08 ± 0.01	6.85 ± 1.80	85.62
3g	3.82 ± 0.20	17.62 ± 0.46	4.61
3h	1.80 ± 0.30	17.33 ± 1.77	9.63
3i	0.51 ± 0.02	>25	>49.02
3j	0.08 ± 0.01	8.00 ± 1.06	100
3k	0.63 ± 0.05	6.20 ± 1.19	9.84
3l	0.34 ± 0.04	>25	>73.53
3m	0.82 ± 0.03	>25	>30.49
3n	3.15 ± 0.21	18.41 ± 1.66	5.84
3o	3.82 ± 0.20	17.62 ± 0.46	4.61
Miltefosine	0.52 ± 0.004	7.69 ± 0.63	14.79

[a] The half-maximal effective concentration (EC_{50}) is defined as that causing a 50% reduction of proliferation in *L. infantum* amastigotes or human THP-1 cells. Dead parasites were identified by their increased permeability to propidium iodide.
[b] The half-maximal lethal concentration (LC_{50}) is defined as that causing a 50% reduction of proliferation in THP-1 monocytes. Dead cells were identified by their increased permeability to propidium iodide.
[c] Selectivity index (SI) is the ratio of LC_{50} values of compounds against THP-1 cells relative to EC_{50} valuesagainst *L. infantum* amastigotes.

2.2.1. Activity in infected macrophages

The four compounds showing EC_{50} values against *L. infantum* axenic amastigotes below 0.2 μM and SI values over 50 were selected for their analysis against intracellular amastigotes. As shown in Table 3, the EC_{50} values obtained for compounds **3c, 3e**, **3f** and **3j** are all in the low micromolar range with the highest activity seen for **3f** (EC_{50} = 1.23 μM). The EC_{50} value obtained for miltefosine was 0.55 μM. These values are 15–40 times higher than those observed for axenic amastigotes except for **3c** whose EC_{50} value is 200 times higher in intracellular amastigotes. This diminished leishmanicidal activity against intracellular amastigotes compared to that observed against axenic amastigotes has been reported by other groups. These different susceptibilities might be explained by a reduced capacity of these compounds to cross host cell membranes or as a consequence of being metabolized by the macrophages [17]. In addition, the higher replication rate of axenic amastigotes compared to that of intracellular amastigotes and their inherent differences in the gene expression profile could also

Table 3
Leishmanicidal activity for selected compounds from series **3** in *L. infantum* amastigote-infected THP-1-derived macrophages.

Compound	EC_{50} (μM)
3c	4.02 ± 1.03
3e	3.10 ± 0.76
3f	1.23 ± 0.17
3j	1.78 ± 0.29
Miltefosine	0.55 ± 0.06

contribute to the different antileishmanial activities obtained in both amastigote models [18].

2.2.2. Inhibition of LiTryR

In an attempt to investigate a possible mechanism of action, the ability of all series **3** compounds to inhibit *Li*TryR was evaluated at a fixed drug concentration of 25 μM. Those molecules that showed inhibitory activity at this concentration and also good EC_{50} values against axenic amastigotes were selected for determination of their IC_{50} in an oxidoreductase assay catalyzed by recombinant *Li*TryR (Table 4). The best IC_{50} values were obtained for compounds **3b** and **3f** (1.85 μM and 2.98 μM, respectively).

Because of its good EC_{50} (amastigote infection assay) and IC_{50} (*Li*TryR activity assay) values, compound **3f** was selected for further characterization of its mode of inhibition. Initial reaction rates were plotted against increasing concentrations of oxidized trypanothione (TS_2) in the presence of **3f** concentrations ranging from 1.25 μM to 20 μM (Fig. 1).

The data obtained could be fitted neither to a linear competitive nor to a linear mixed inhibition model. On the contrary, our data nicely fit to a hyperbolic noncompetitive inhibition model (Fig. 1), in which a partially productive enzyme/substrate/inhibitor complex (ESI complex) is formed. The inhibition constant (K_i) for the binding of compound **3f** to the TS_2-depleted enzyme has a value of 2.83 ± 0.70 μM. The inhibitor may also bind to the enzyme/substrate (ES) complex showing a slightly higher dissociation constant ($\alpha = 1.27 \pm 0.37$; Scheme 2). The nonlinear behavior of this inhibition is due to the ability of the ESI complex to generate reduced trypanothione ($T(SH)_2$) but with a highly reduced catalytic efficiency compared to ES ($\beta = 0.23 \pm 0.03$; Scheme 2).

As shown in Scheme 2, *Li*TryR can form a ternary complex with TS_2 and **3f** that can yield $T(SH)_2$ much less readily than the binary *Li*TryR/TS_2 complex does. Contrary to classical inhibitions in which the ternary complex is unable to yield product ($\beta = 0$), in the inhibition caused by **3f** the apparent values of K_m/V_{max}^{app} (slope in the double reciprocal plots) and $1/V_{max}^{app}$ (intercept in the double reciprocal plots) display a nonlinear dependence on the inhibitor concentration which is described by a hyperbolic function (Fig. 2) [19].

Since the enzymatic reaction catalyzed by *Li*TryR is a bi−bi reaction, the effect of varying NADPH concentration (at a saturating TS_2 concentration) on **3f** inhibition was also evaluated. Initial reaction rates were plotted against increasing NADPH concentrations in the presence of different **3f** concentrations (Fig. 3A). Our data nicely fit to a hyperbolic uncompetitive inhibition, in which the inhibitor binds only to the enzyme/substrate complex (*Li*TryR/NADPH) (Scheme 3). Accordingly, the K_i for the binding of compound **3f** to the enzyme/substrate complex has a value of 1.37 ± 0.16 μM. The series of lines observed in the Lineweaver-Burk double-reciprocal plot are not completely parallel because of the slight activity of the ESI complex that is characteristic of hyperbolic inhibition. As expected for an uncompetitive mode of inhibition, their intercepts with the y- and x-axis indicate that the apparent values of V_{max} and K_m decrease with increasing inhibitor concentrations (Fig. 3B).

Only a few cases uncompetitive inhibitors versus NADPH have been described for TryR [20,21]. In enzymes, such as this one, that obey a bi-bi reaction mechanism, an uncompetitive pattern can arise due to competition of the inhibitor for the second independent substrate-binding site, TS_2 site in this case. However, the noncompetitive inhibition pattern that was observed when the concentration of TS_2 was varied in the presence of a fixed concentration of NADPH suggests that either **3f** is able to bind to the TS_2 site in the presence of TS_2 or it binds to a site that is different from any of the two substrate-binding sites. A disruption of the orientation or even displacement of FAD has been proposed for NADPH uncompetitive inhibitors of TryR containing a pyrimidopyridazine scaffold [21]. Alternatively, binding to the interface between both subunits of TryR was suggested for some nitrofurans that also behave as uncompetitive inhibitors for NADPH [20]. Similar to **3f** in *Li*TryR, nitrofurans with aromatic and heterocyclic substituents have been shown to inhibit TryR from *Trypanosoma congolense* acting as uncompetitive inhibitors versus NADPH and noncompetitive inhibitors versus TS_2. Moreover, these compounds are responsible for the TryR-dependent reduction of cytochrome *c* in a reaction that may be inhibited by superoxide dismutase, a finding that points to generation of superoxide anion during the process [20]. Based on the similar kinetic behavior of **3f** to that described for nitrofurans, we evaluated the putative reduction of cytochrome *c* by *Li*TryR in the presence of **3f** using menadione as a positive control either in the presence or in the absence of superoxide dismutase. The results shown in Fig. 4 reveal a much higher capacity of **3f** for cytochrome *c* reduction than that observed for menadione. This reduction is mediated by superoxide anion generation in the *Li*TryR-catalyzed enzymatic reaction, as demonstrated by the strong decrease in the concentration of reduced cytochrome *c* in the presence of superoxide dismutase (filled diamonds vs empty diamonds).

The introduction of different substituents onto the π-deficient pyridazino-pyrrolo-quinoxalinium aromatic scaffold is shown to modulate the disulfide reduction inhibitory properties of the present compounds. Menadione and other related 1,4-naphthoquinones are known to behave as redox cyclers or "subversive substrates" for several NADPH-dependent disulfide reductases, including TryR [22]. In the presence of oxygen, reoxidation of the reduced molecule following one- or two-electron transfer reactions leads to both a steady flux of reactive oxygen species and NADPH consumption [22,23]. For these reasons, we thought of interest to compare the energies of the lowest-unoccupied molecular orbitals of menadione and **3f**, as well as their atomic contributions. The finding that the respective LUMO energies are −3.108 eV and −3.071 eV strongly suggests that both electron-deficient molecules display similar electron-accepting properties. Furthermore, it can be seen that the largest contributions to the LUMO of **3f** (Fig. 5) arise from the quinone system and pyridazine ring atoms, respectively. In addition, the predicted redox potential for **3f** (−0.681 V) using the web server available on http://infochim.u-strasbg.fr/cgi-bin/predictor.cgi compares favorably to that calculated for menadione (−0.604 V). Taken together, these results support the view that **3f** also behaves as a "subversive substrate" for *Li*TryR.

Table 4
Activity of selected compounds from series 3 against *Li*TryR.

Compound	IC_{50}[a] (μM)
3b	1.85 ± 0.23
3d	7.92 ± 0.28
3e	25.66 ± 2.33
3f	2.98 ± 0.71
3k	13.91 ± 1.49
3l	6.90 ± 1.33
3o	23.60 ± 0.81
Mepacrine[b]	13.53 ± 1.18

[a] Half-maximal inhibitory concentration (IC_{50}) ± standard error (SE) values for selected compounds from series **3** in the *Li*TryR oxidoreductase activity assay. Results are representative of three independent experiments.
[b] Mepacrine was included as the reference compound.

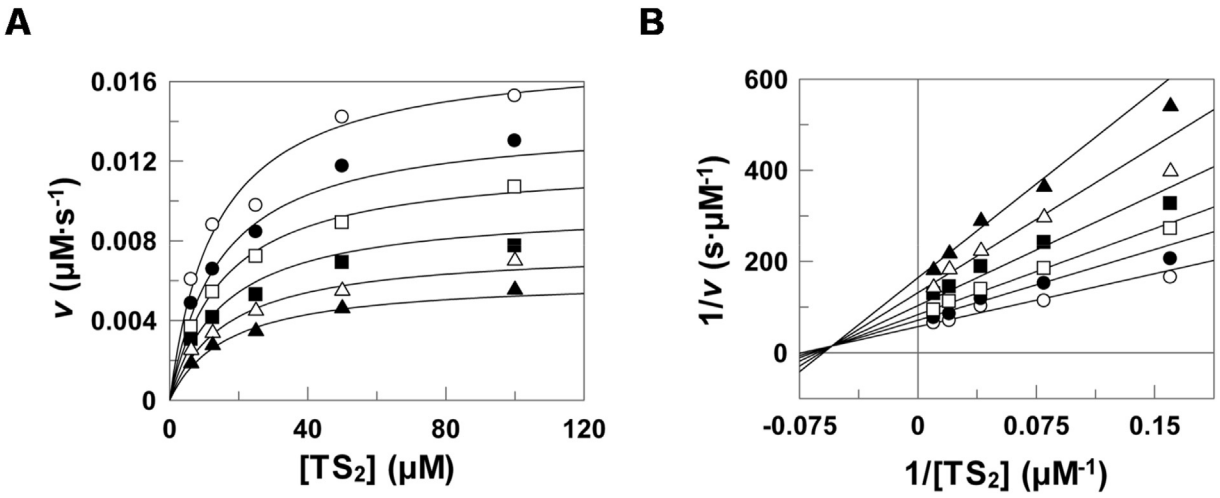

Fig. 1. Noncompetitive hyperbolic inhibition of *Li*TryR by 3f. (A) Plot of the initial velocities as a function of TS_2 concentration at six different **3f** concentrations: 0 (○), 1.25 (●), 2.5 (□), 5 (■), 10 (Δ) and 20 (▲) μM. 2-nitro-5-thiobenzoic acid (TNB) production was monitored by the increase in absorbance at 412 nm. Curves were fitted using Equation 4. (B) Double-reciprocal plot. Data are the results obtained in a representative assay from three independent experiments.

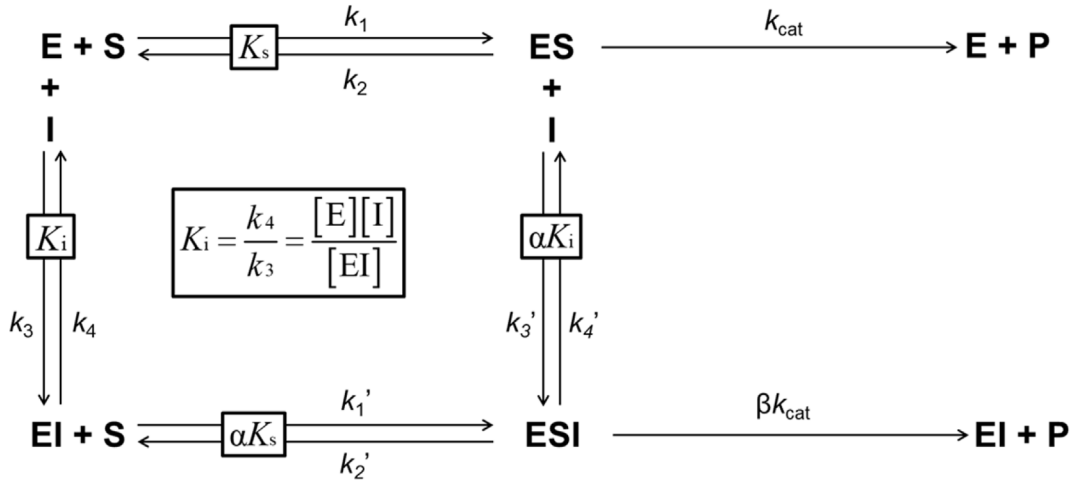

Scheme 2. Hyperbolic mixed inhibition of *Li*TryR by **3f** in the presence of saturating concentrations of NADPH. The inhibitor binds both to the free (E) and TS_2-bound (ES) forms of the enzyme. The ESI complex is able to catalyze TS_2 reduction but at a much slower rate than the ES complex does.

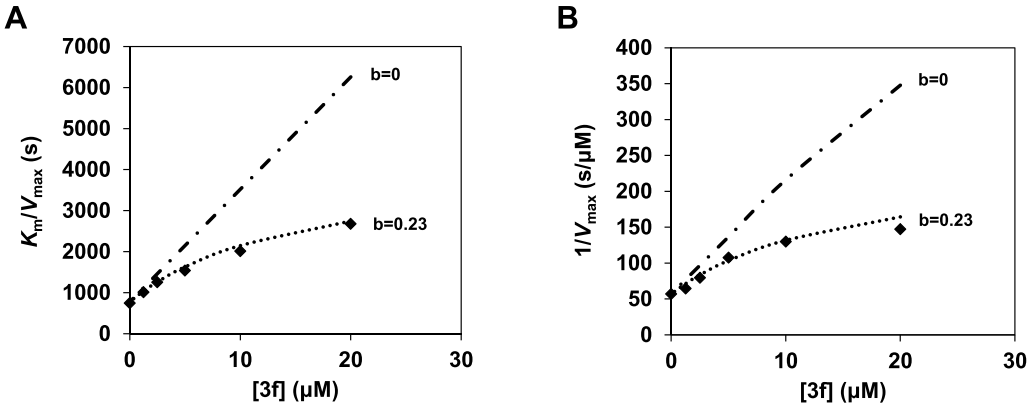

Fig. 2. Nonlinear dependence of the apparent values of K_m/V_{max}^{app} and $1/V_{max}^{app}$ functions on 3f concentration. (A) Replot of slopes (K_m/V_{max}^{app}) from Fig. 1B as a function of increasing **3f** concentrations. (B) Replot of y-intercepts ($1/V_{max}^{app}$) from Fig. 1B as a function of increasing **3f** concentrations. The theoretical plot for a linear inhibitor ($\beta = 0$) is included. Experimental values fit to a hyperbolic inhibition with a β value of 0.23 (Equations (5) and (6)). Data are the results obtained in a representative assay from three independent experiments.

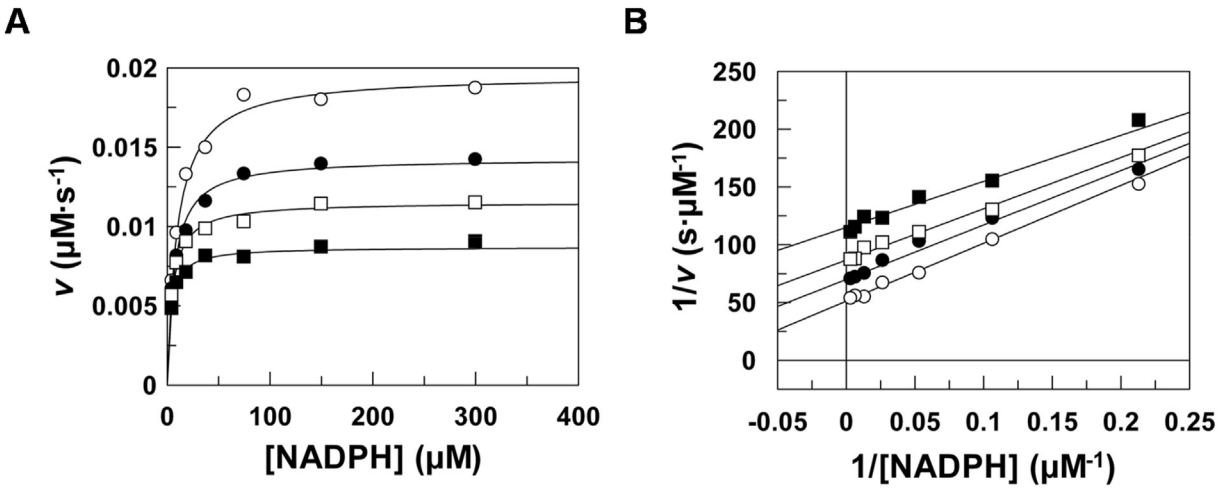

Fig. 3. Uncompetitive hyperbolic inhibition of *Li*TryR by 3f. (A) Plot of the initial velocities as a function of NADPH concentration at four different **3f** concentrations: 0 (○), 0.625 (●), 1.25 (□), and 2.5 (■) μM. TNB production was monitored by the increase in absorbance at 412 nm. Curves were fitted using Equation 4. (B) Double-reciprocal plot. Data are the results obtained in a representative assay from three independent experiments.

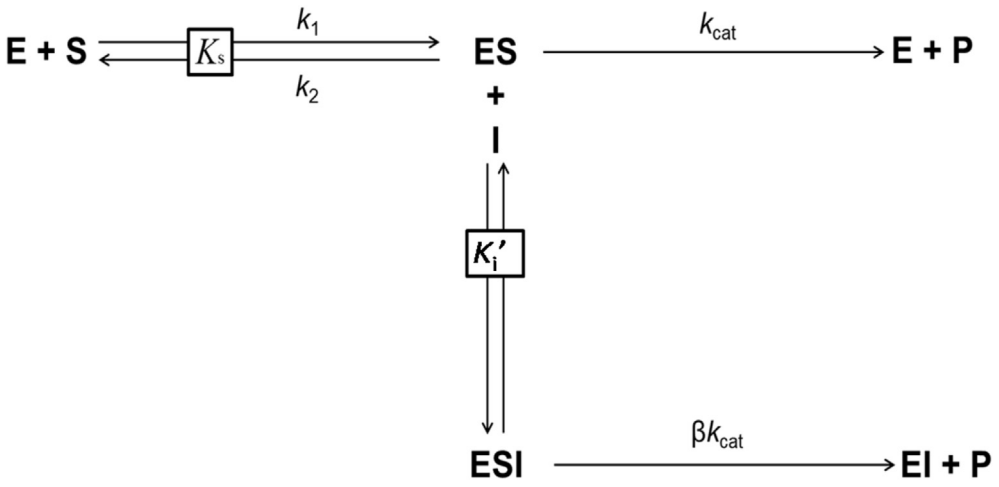

Scheme 3. Hyperbolic uncompetitive inhibition of *Li*TryR by **3f** in the presence of saturating concentrations of TS_2. The inhibitor only binds to the NADPH-bound (ES) form of the enzyme. The ESI complex is able to catalyze TS_2 reduction but at a much slower rate than the ES complex does.

3. Conclusions

Based on our previous experience in the synthesis of pyrroloquinoxaline derivatives, fifteen compounds modified at four different positions on the pyridazino[2,3-*a*]pyrrolo[2,1-*c*]quinoxal-13-inium scaffold were prepared and evaluated as leishmanicidal agents. Eleven of them display submicromolar activity against axenic amastigotes and low cytotoxicity against THP-1 cells, which gives rise to a four-digit SI value for compound **3c**. Highly relevant is the potent leishmanicidal activity exhibited by compound **3f** on intracellular amastigotes, which is very close to that observed for the reference drug miltefosine. This compound potently inhibits *Li*TryR and thereby targets the trypanothione-based antioxidant system that is essential for these parasites. It displays a hyperbolic noncompetitive behavior versus TS_2 and a hyperbolic uncompetitive behavior versus NADPH. Similar to other uncompetitive TryR inhibitors, compound **3f** behaves as a "subversive substrate" for *Li*TryR that not only alters the physiological reduction of TS_2, but also converts this antioxidant oxidoreductase in a prooxidant enzyme that produces superoxide anion through a futile consumption of NADPH and O_2. These two activities are highly relevant for inducing severe alterations in the redox homeostasis of *Leishmania* parasites and causing cell death.

Altogether, these results reveal that pyridazino-pyrroloquinoxalinium salts may be considered as promising candidates for further development of leishmanicidal drugs targeting TryR. Furthermore, our results provide the first evidence of a pyridazinopyrrolo-quinoxalinium salt that behaves as a "subversive substrate" for TryR. As already described for other TryR subversive substrates, the precise binding site of compound **3f** in *Li*TryR has not yet been defined and additional experiments are in course to allocate it.

4. Experimental

4.1. Chemistry

Solvents (HPLC quality, Scharlau) were dried in a Solvent Purification System (MBraun) by passing through a pre-activated alumina column or were purchased as anhydrous quality. Reagents were purchased from Sigma-Aldrich or Acros and were used as received. The reactions in which moisture-sensitive compounds were handled were performed under an atmosphere of dry argon.

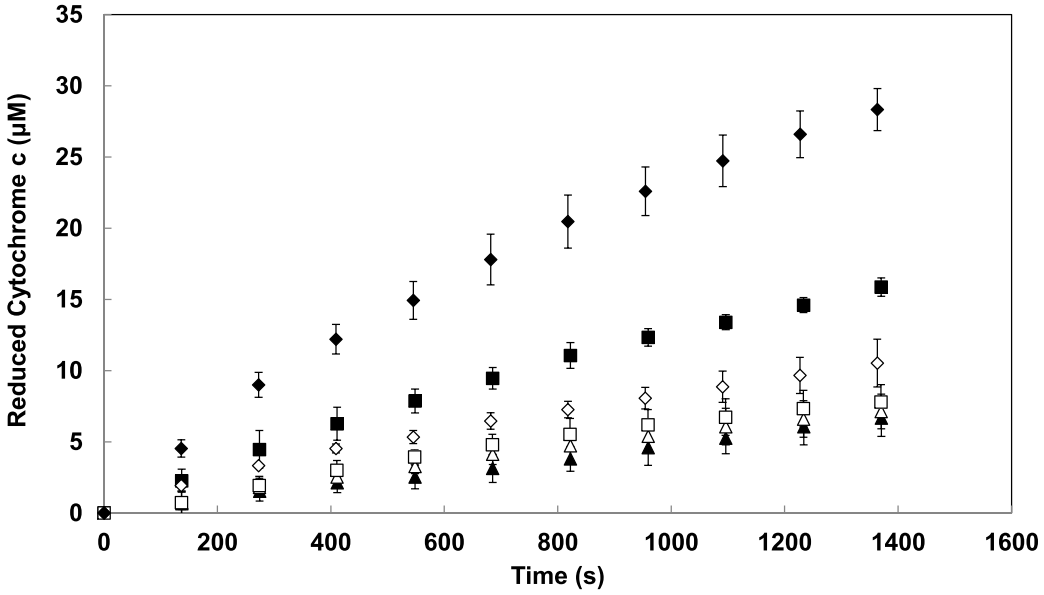

Fig. 4. ***Li*TryR-mediated cytochrome *c* reduction**. The increase in the reduced cytochrome *c* concentration as a consequence of *Li*TryR activity was evaluated in the presence of DMSO as vehicle (triangles), 10 μM menadione (squares) and 10 μM **3f** (diamonds) and in the absence (filled symbols) or in the presence (empty symbols) of *L. infantum* superoxide dismutase A (4 μM).

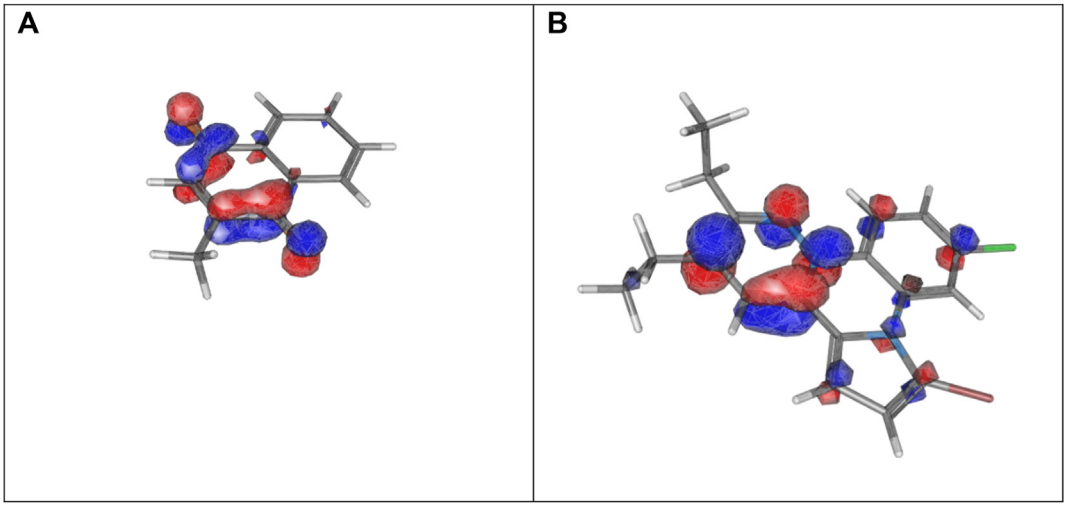

Fig. 5. Optimized geometries and lowest unoccupied molecular orbitals of (A) neutral menadione and (B) positively charged **3f.**

The reactions performed at low temperature were carried out using a cryostat *Haake* EK 101. The reactions were monitored by thin-layer chromatography (TLC) on silica-coated aluminum sheets (Alugram silica gel 60 F_{254}). The compounds were visualized by UV light (254 nm). Column chromatography was carried out with Merck silica gel (0.030–0.075 mm) and the solvents were used as received (Scharlau). Infrared spectra (IR, NaCl windows or KBr pellets) were recorded on a PerkinElmer FTIR 1725X instrument. The frequencies (ν) of the more intense bands are given in cm^{-1}. Nuclear magnetic resonance spectra (^1H and ^{13}C NMR) were recorded using a Varian Gemini 200 (200 and 50 MHz, respectively), a Varian UNITY-300 (300 and 75 MHz, respectively); a Varian Mercury-VX-300 MHz and a Varian-UNITY^{PLUS}-500 (500 and 125 MHz, respectively) instrument. Chemical shifts (δ) are given in ppm and are referenced to the residual signal of the non-deuterated solvent. Coupling constants (J) are given in Hz. Final compounds were purified by crystallization and melting points values were within 1 °C to 2 °C range. Compounds were pure by H NMR. High-resolution mass spectra were recorded on an Agilent 6210 LC/MS TOF mass spectrometer.

4.1.1. Synthesis of pyridazino[2,3-a]pyrrolo[2,1-c]quinoxalinium salts

Method A: To a solution of 2 (0.19–0.37 eq.) in ethanol (0.1 mL/mmol), butane-2,3-dione (1 equiv) and Et_3N (1 equiv) were added, and the reaction mixture was stirred at room temperature. The solvent was removed under reduced pressure and the residue was treated with Et_2O to give a solid. After filtration, the solid was crystallized in EtOH/AcOEt.

Method B: To a solution of **2** (0.19–0.3 mmol) in ethanol (0.1 mL/

mmol), 1,4-dioxane-2,3-diol (1.1 equiv) and Et_3N (1.1 equiv) were added. The reaction mixture was heated at reflux temperature. The solvent was removed under reduced pressure and the residue was treated with Et_2O to give a solid. After filtration, the solid was crystallized in EtOH/AcOEt.

Method C: To a solution of **2** (0.18 mmol) in acetone (0.1 mL/mmol), acenaphthoquinone (1.1 equiv) and AcONa (1.1 equiv) were added. The reaction mixture was heated at reflux temperature for 4 h. The solvent was removed under reduced pressure and the residue was treated with Et_2O to give a solid. After filtration, the solid was crystallized in EtOH/AcOEt.

Method D: To a solution of **2** (0.23 mmol) in MeOH (0.42 mL/mmol), hexane-3,4-dione (1.1 equiv) and Et_3N (1.1 equiv) were added. The reaction mixture was heated at reflux temperature for 3 h. The solvent was removed under reduced pressure and the residue was treated with Et_2O to give a solid. After filtration, the solid was crystallized in MeOH/Et_2O.

Method E: To a solution of **2** (0.23–0.36 mmol) in MeOH (30 mL/mmol), hexane-3,4-dione (2 equiv) and Et_3N (1 equiv) were added. The reaction mixture was heated at reflux temperature. The precipitate obtained was filtered off and washed with MeOH.

*4.1.2. 8H-2,3-Dimethylpyridazino[2,3-a]pyrrolo[2,1-c]quinoxal-13-inium mesitylenesulfonate (**3a**)*

Method A from **2a** (145 mg; 0.37 mmol) for 20 min. Yield: 59.7 mg (0.13 mmol, 34%); Greenish solid; mp: 215–216 °C; ^{1}H NMR (300 MHz, CD_3OD) δ 8.90 (dd, 1H, J = 8.5 Hz, J = 1.2 Hz), 8.79 (s, 1H), 8.65 (dd, 1H, J = 2.6 Hz, J = 1.2 Hz), 8.36 (d, 1H, J = 8.5 Hz), 8.00–7.83 (m, 2H), 7.75 (dt, 1H, J = 8.5 Hz, J = 1.2 Hz), 7.21 (dd, 1H, J = 4.4 Hz, J = 2.6 Hz), 6.69 (s, 2H), 2.84 (s, 3H), 2.70 (s, 3H), 2.53 (s, 6H), 2.12 (s, 3H) ppm; ^{13}C NMR (75 MHz, CD_3OD) δ 161.4, 147.9, 140.8, 139.8, 139.4, 138.0, 133.4, 131.5 (2C), 128.9 (2C), 128.8, 128.5, 128.1, 123.4, 121.5, 121.4, 118.3, 117.5, 116.6, 23.3 (2C), 20.8, 20.6, 19.5 ppm; IR (KBr) ν 3448.1, 3080.7, 1732.7, 1629.4, 1606.0, 1555.7, 1499.0, 1483.4, 1395.9, 1335.5, 1250.6, 1190.8, 1083.5, 1014.1, 918.7, 876.7, 848.7, 764.9, 676.1, 640.2, 579.8, 547.8, 527.5, 482.2 cm^{-1}; HRMS (ESI$^+$): *m/z* calcd. for $C_{16}H_{14}N_3$, 248.1188; found, 248.1163.

*4.1.3. 4H-Acenaphtho[1′,2′:3,4]pyridazino[2,3-a]pyrrolo[2,1-c]quinoxal-9-inium mesitylenesulfonate (**3b**)*

Method C from **2a** (73.6 mg; 0.18 mmol). Yield: 61.3 mg (0.11 mmol, 62%); Orange solid; mp: 327–328 °C. ^{1}H NMR (300 MHz, CD_3OD) δ 9.49 (s, 1H), 9.02 (d, 1H, J = 8.9 Hz), 8.72 (bs, 1H), 8.56 (d, 1H, J = 6.9 Hz), 8.52 (d, 1H, J = 7.2 Hz), 8.38 (d, 1H, J = 7.9 Hz), 8.26 (t, 2H, J = 7.4 Hz), 8.12 (d, 1H, J = 3.9 Hz), 8.05–7.85 (m, 3H), 7.79 (t, 1H, J = 7.9 Hz), 7.31 (q, 1H, J = 3.4 Hz), 6.85 (s, 2H), 2.62 (s, 6H), 2.24 (s, 3H) ppm; ^{13}C NMR (75 MHz, CD_3OD) δ 157.8, 140.8, 140.1, 138.5, 138.2 (2C), 133.7, 133.4, 133.0, 131.6 (2C), 131.4, 130.8, 130.6, 130.1, 129.5, 128.9 (2C), 128.7, 128.5, 127.9, 125.4, 123.9, 123.0, 121.4, 120.4, 118.9, 117.6, 117.2, 23.3 (2C), 20.8 ppm; IR (KBr) ν 3424.3, 3090.9, 1631.0, 1605.4, 1543.7, 1482.2, 1445.6, 1419.3, 1212.0, 1196.2, 1085.4, 1017.0, 951.9, 852.2, 833.8, 781.2, 768.5, 675.8, 585.2, 550.3 cm^{-1}; HRMS (ESI-TOF): *m/z* calcd. for $C_{24}H_{14}N_3$, 344.1182; found, 344.1197.

*4.1.4. 10-Chloro-8H-pyridazino[2,3-a]pyrrolo[2,1-c]quinoxal-13-inium mesitylenesulfonate (**3c**)*

Method B from **2b** (122.0 mg; 0.28 mmol) for 20 min. Yield: 60.3 mg (0.132 mmol, 47%); Dark-green solid; mp: 275–276 °C. ^{1}H NMR (300 MHz, CD_3OD) δ 9.26 (dd, 1H, J = 4.2 Hz, J = 1.3 Hz, H-2), 9.15 (dd, 1H, J = 8.9 Hz, J = 1.3 Hz, H-4), 8.97 (d, 1H, J = 9.4 Hz, H-12), 8.85 (d, 1H, J = 2.5 Hz, H-7), 8.66 (d, 1H, J = 2.1 Hz, H-9), 8.27 (dd, 1H, J = 8.9 Hz, J = 4.7 Hz, H-3), 8.16 (d, 1H, J = 4.2 Hz, H-5), 7.84 (dd, 1H, J = 9.4 Hz, J = 2.1 Hz, H-11), 7.35 (t_{app}, 1H, J = 3.6 Hz, H-6), 6.85 (s, 2H, $H_{Ar\text{-}MSTS}$), 2.61 (s, 6H, $CH_{3\text{-}MSTS}$), 2.24 (s, 3H, $CH_{3\text{-}MSTS}$) ppm; ^{13}C NMR (75 MHz, CD_3OD) δ 150.5, 141.1, 140.8, 140.1, 140.0, 138.2, 133.4, 131.8, 131.6 (2C), 130.1, 129.1 (2C), 127.6, 124.9, 123.5, 122.5, 119.2, 118.1, 117.9, 23.3 (2C), 20.8 ppm; IR (KBr) ν 3422.3, 3091.1, 1623.3, 1605.6, 1557.7, 1535.0, 1497.0, 1472.9, 1431.8, 1189.2, 1086.1, 1016.0, 848.7, 810.3, 752.4, 678.8, 851.4 cm^{-1}; HRMS (ESI$^+$): *m/z* calcd. for $C_{14}H_9ClN_3$, 254.0480; found, 254.0479.

*4.1.5. 10-Chloro-8H-2,3-dimethylpyridazino[2,3-a]pyrrolo[2,1-c]quinoxal-13-inium mesitylenesulfonate (**3d**)*

Method A from **2b** (116.9 mg; 0.27 mmol) for 30 min. Yield: 54.5 mg (0.11 mmol, 42%); Black solid; mp: 231–232 °C; ^{1}H NMR (300 MHz, CD_3OD) δ 8.90 (d, 1H, J = 9.2 Hz, H-12), 8.83 (s, 1H, H-4), 8.68 (dd, 1H, J = 2.6 Hz, J = 1.3 Hz, H-7), 8.53 (s, 1H, H-9), 7.99 (d, 1H, J = 4.3 Hz, H-5), 7.75 (dd, 1H, J = 9.2 Hz, J = 1.6 Hz, H-11), 7,24 (t_{app}, 1H, J = 3.4 Hz, H-6), 6.72 (s, 2H, $H_{Ar\text{-}MSTS}$), 2.87 (s, 3H, CH_3), 2.73 (s, 3H, CH_3), 2.62 (s, 6H, $CH_{3\text{-}MSTS}$), 2.24 (s, 3H, $CH_{3\text{-}MSTS}$) ppm; ^{13}C NMR (75 MHz, CD_3OD) δ 161.6, 148.2, 140.8, 139.8, 139.5, 139.3, 138.1, 131.5 (2C), 129.7, 129.1, 128.7 (2C), 127.0, 123.9, 123.2, 121.9, 118.6, 117.6, 117.0, 23.3 (2C), 20.8, 20.5, 19.5 ppm; IR (KBr) ν 3422.4, 3076.1, 1735.1, 1602.8, 1556.7, 1472.4, 1432.1, 1248.6, 1178.3, 1084.2, 1013.0, 843.4, 827.1, 769.1, 676.8, 606.9, 578.9 cm^{-1}; HRMS (ESI$^+$): *m/z* calcd. for $C_{16}H_{13}ClN_3$, 282.0793; found, 282.0795.

*4.1.6. Ylide **4b** and 10-chloro-2,3-diethyl-8H-pyridazino[2,3-a]pyrrolo[2,1-c]quinoxal-13-inium bromide (**3e**)*

Method E from **2b** (0.36 g; 0.84 mmol) for 4 h. Then, 46% HBr (47 μL, 0.42 mmol) was added on a slurry of **4b** (0.13 g; 0.42 mmol) in H_2O (9 mL) at 0 °C and the mixture was stirred for 10 min. Next, the mixture was stirred at room temperature for 3.75 h to give a precipitate which was filtered off. Finally, the filtrate was lyophilized.

*Compound **4b***: Yield: 0.16 g (0.51 mmol, 61%); Ochre solid; mp: 157–158 °C; ^{1}H NMR (300 MHz, $CDCl_3$): δ 7.85 (d, 1H, J = 8.8 Hz, H-12), 7.36 (d, 1H, J = 2.0 Hz, H-9), 7.26 (bs, 2H, H-4, H-7), 7.09 (dd, 1H, J = 9.1 Hz, J = 2.0 Hz, H-11), 6.61 (d, 1H, J = 3.8 Hz, H-5), 6.49 (t_{app}, 1H, J = 3.8 Hz, J = 2.9 Hz, H-6), 4.99 (q, 1H, J = 7.3 Hz, CH), 2.43 (q, 2H, J = 7.3 Hz, CH_2), 1.71 (d, 3H, J = 7.2 Hz, CH–CH_3), 1.26 (t, 3H, J = 7.5 Hz, CH_2–CH_3) ppm; ^{13}C NMR (75 MHz, $CDCl_3$) δ 169.5, 162.0, 138.5, 132.5, 126.8, 126.1, 125.5, 120.8, 119.7, 117.2, 116.8, 114.8, 114.7, 110.2, 105.0, 29.7, 23.9, 10.4 ppm; IR (KBr) ν 3419.0, 3108.4, 2970.9, 2359.6, 1606.7, 1503.4, 1434.4, 1363.9, 1305.4, 1154.9, 1100.1, 1034.6, 843.5, 810.2 cm^{-1}; HRMS (ESI-TOF): *m/z* calcd. for $C_{18}H_{17}ClN_3$, 310.1106; found, 310.1089.

*Compound **3e***: Yield: 68.5 mg (0.175 mmol, 41%); Orange solid; mp: 251–252 °C; ^{1}H NMR (200 MHz, CD_3OD): δ 9.00 (d, 1H, J = 9.3 Hz, H-12), 8.81 (s, 1H, H-4), 8.78 (d, 1H, J = 2.5 Hz, H-7), 8.65 (d, 1H, J = 2,1 Hz, H-9), 8.17 (d, 1H, J = 4.2 Hz, H-5), 7.83 (dd, 1H, J = 9.3 Hz, J = 1.7 Hz, H-11), 7.30 (t_{app}, 1H, J = 3.4 Hz, H-6), 3.25 (q, 2H, J = 7.2 Hz, CH_2), 3.09 (q, 2H, J = 7.6 Hz, CH_2), 1.61 (t, 3H, J = 7.2 Hz, CH_3), 1.53 (t, 3H, J = 7.6 Hz, CH_3) ppm; ^{13}C NMR (75 MHz, CD_3OD): δ 144.4, 140.8, 139.9, 138.7, 138.1, 131.6, 128.9, 126.8, 126.1, 122.8, 121.1, 118.1, 117.6, 115.8, 20.8, 20.5, 20.2, 20.0 ppm; IR (KBr) ν 3415.1, 3025.2, 2970.4, 2932.4, 1619.7, 1601.5, 1551.3, 1473.8, 1428.5, 1375.7, 1246.7, 1160.7, 1101.8, 1051.1, 911.9, 886.6, 777.9, 698.3, 650.7 cm^{-1}; HRMS (ESI-TOF): *m/z* calcd. for $C_{18}H_{17}ClN_3$, 310.1106; found, 310,1093.

*4.1.7. Ylide **4c** and 7-bromo-10-chloro-2,3-diethyl-8H-pyridazino[2,3-a]pyrrolo[2,1-c]quinoxal-13-inium bromide (**3f**)*

Method E from **2c** (0.23 g, 0.45 mmol) for 3 h. Next, 46% HBr (15 μL, 0.42 mmol) was added on a solution of **4c** (52.3 mg, 0.13 mmol) in CH_2Cl_2 (12 mL) at 0 °C and the reaction mixture was stirred for 10 min. Then, the mixture was stirred at room temperature for 6.5 h and the solvents were evaporated to dryness. The residue was treated with Et_2O to give a solid which was filtered off.

Compound ***4c***: Yield: 0.14 g (0.36 mmol, 80%); Yellow solid; mp: 211–212 °C; ^{1}H NMR (200 MHz, $CDCl_3$): δ 8.75 (s, 1H), 7.85 (d, 1H, *J* = 8.9 Hz), 7.11 (d, 1H, *J* = 8.9 Hz), 6.58 (d, 1H, *J* = 3.8 Hz), 6.48 (d, 1H, *J* = 3.4 Hz), 5.88 (s, 1H), 4.98 (q, 1H, *J* = 7.2 Hz), 2.40 (q, 2H, *J* = 7.0 Hz), 1.69 (d, 3H, *J* = 7.2 Hz), 1.24 (t, 3H, *J* = 7.0 Hz) ppm; ^{13}C NMR (50 MHz, $CDCl_3$): δ 154.9, 126.7, 126.0, 125.9, 125.7, 124.7, 118.6, 115.9, 115.6, 110.5, 106.2, 104.8, 103.9, 97.8, 93.6, 25.5, 12.6, 10.2 ppm; IR (KBr) ν 3424.0, 2971.6, 2908.9, 2348.3, 1639.1, 1493.4, 1387.4, 1311.8, 1104.8, 1041.9, 977.8, 847.2, 818.2, 802.2, 764.9, 749,2 cm^{-1}; HRMS (ESI-TOF): *m/z* calcd. for $C_{18}H_{16}^{79}BrClN_3$ $[M+1]^+$, 388.0211; found 388.0170.

Compound ***3f***: Yield: 61.1 mg (0.13 mmol, 97%); Yellow solid; mp: 200–202 °C; ^{1}H NMR (300 MHz, CD_3OD): δ 9.61 (d, 1H, *J* = 2.0 Hz, H-9), 9.11 (d, 1H, *J* = 9.4 Hz, H-12), 8.82 (s, 1H, H-4), 8.26 (d, 1H, *J* = 4.7 Hz, H-5/H-6), 7.92 (dd, 1H, *J* = 9.4 Hz, *J* = 2.0 Hz, H-11), 7.41 (d, 1H, *J* = 4.7 Hz, H-6/H-5), 3.27 (q, 2H, *J* = 7.3 Hz, CH_2), 3.09 (q, 2H, *J* = 7.3 Hz, CH_2), 1.60 (t, 3H, *J* = 7.3 Hz, CH_3), 1.53 (t, 3H, *J* = 7.3 Hz, CH_3) ppm; ^{13}C NMR (75 MHz, CD_3OD): δ 164.3, 153.0, 138.9, 137.9, 130.9, 129.2, 128.3, 126.7, 124.7, 124.3, 123.3, 118.0, 117.8, 109.5, 27.4, 26.0, 12.3, 10.9 ppm; IR (KBr) ν 3422.5, 3022.7, 2930.5, 2363.5, 1623.8, 1599.8, 1552.0, 1471.8, 1397.3, 1373.0, 1253.4, 1100.3, 1053.0, 975.8, 932.1, 849.6, 840.5, 799.8, 780.4, 652.4 cm^{-1}; HRMS (ESI-TOF): *m/z* calcd. for $C_{18}H_{16}^{81}BrClN_3$ $[M+2]^+$, 390.0189; found, 390.0185.

4.1.8. 8H-2,3,11-Trimethylpyridazino[2,3-a]pyrrolo[2,1-c]quinoxal-13-inium mesitylenesulfonate (*3g*)

Method A from **2d** (124.0 mg, 0.30 mmol) for 20 min. Yield: 68 mg (0.139 mmol, 46%); Greenish solid; mp: 146–147 °C; ^{1}H NMR (300 MHz, CD_3OD): δ 8.79 (s, 1H), 8.72 (s, 1H), 8.62 (s, 1H), 8.25 (d, 1H, *J* = 8.6 Hz), 7.94 (d, 1H, *J* = 4.3 Hz), 7.75 (d, 1H, *J* = 8.6 Hz), 7.21 (t, 1H, *J* = 2.9 Hz), 6.73 (s, 2H), 2.85 (s, 3H), 2.71 (s, 3H), 2.63 (s, 3H), 2.55 (s, 6H), 2.15 (s, 3H) ppm; ^{13}C NMR (75 MHz, CD_3OD): δ 161.2, 147.6, 140.8, 139.9, 139.5, 139.3, 138.1, 134.4, 131.5 (2C), 128.9 (2C), 127.9, 126.7, 123.1, 121.4, 120.9, 118.2, 117.3, 116.2, 23.3 (2C), 21.4, 20.8, 20.5, 19.5 ppm; IR (KBr) ν 3432.4, 2918.0, 1735.9, 1629.9, 1603.5, 1553.6, 1509.0, 1459.1, 1393.4, 1317.7, 1188.4, 1083.8, 1014.1, 676.2, 581.2 cm^{-1}; HRMS (ESI^+): *m/z* calcd. for $C_{17}H_{16}N_3$, 262.1339; found, 262.1339.

4.1.9. 8H-10,11-Dimethylpyridazino[2,3-a]pyrrolo[2,1-c]quinoxal-13-inium mesitylenesulfonate (*3h*)

Method B from **2e** (130.0 mg, 0.30 mmol) for 20 min. Yield: 78.9 mg (0.176 mmol, 58%); Black solid; mp: 279–280 °C; ^{1}H NMR (300 MHz, CD_3OD): δ 9.22 (s, 1H), 9.11 (d, 1H, *J* = 8.8 Hz), 8.77 (bs, 2H), 8.31 (s, 1H), 8.21 (dd, 1H, *J* = 8.8 Hz, *J* = 3.6 Hz), 8.09 (d, 1H, *J* = 4.1 Hz), 7.32 (m,1H), 6.87 (s, 2H, $H_{Ar\text{-}MSTS}$), 2.64 (s, 6H, 2 $CH_{3\text{-}MSTS}$), 2.63 (s, 3H), 2.58 (s, 3H), 2.25 (s, 3H, $CH_{3\text{-}MSTS}$) ppm; ^{13}C NMR (75 MHz, CD_3OD): δ 15.1, 145.2, 140.8, 140.2, 140.0, 139.1, 138.2, 132.4, 131.7, 131.6 (2C), 127.2 (2C), 126.5, 123.7, 122.1, 121.3, 118.7, 117.8, 116.9, 23.3 (2C), 20.8, 20.3, 20.0 ppm; IR (KBr) ν 3393.8, 3114.7, 3044.0, 1620.4, 1553.6, 1528.6, 1500.3, 1476.8, 1448.5, 1389.1, 1346.1, 1288.5, 1246.3, 1211.3, 1166.2, 1084.7, 1012.3, 911.5, 859.3, 844.6, 830.7, 754.3, 677.1, 583.5 cm^{-1}; HRMS (ESI-TOF): *m/z* calcd. for $C_{16}H_{14}N_3$, 248.1182; found, 248.1179.

4.1.10. 8H-2,3,10,11-Tetramethylpyridazino[2,3-a]pyrrolo[2,1-c]quinoxal-13-inium mesitylenesulfonate (*3i*)

Method A from **2e** (96.1 mg, 0.22 mmol) for 30 min. Yield: 59 mg (0.12 mmol, 56%); Greenish solid; mp: 242–243 °C; ^{1}H NMR (300 MHz, CD_3OD): δ 8.83 (s, 1H, H-4), 8,72 (s, 1H, H-12), 8.65 (s, 1H, H-7), 8.23 (s, 1H, H-9), 7.96 (d, 1H, *J* = 3.2 Hz, H-5), 7.23 (bs, 1H, H-6), 6.82 (s, 2H, $H_{Ar\text{-}MSTS}$), 2.86 (s, 3H, CH_3), 2.71 (s, 3H, CH_3), 2.60 (s, 6H, $CH_{3\text{-}MSTS}$), 2.56 (s, 3H, CH_3), 2.21 (s, 3H, $CH_{3\text{-}MSTS}$) ppm; ^{13}C NMR (75 MHz, CD_3OD): δ 161.1, 147.0, 144.4, 140.8, 139.9, 138.8, 138.7, 138.1, 131.6 (2C), 128.9 (2C), 126.8, 126.1, 122.8, 121.5, 121.1, 118.1, 117.6, 115.8, 23.2 (2C), 20.8, 20.5, 20.2, 20.0, 19.4 ppm; IR (KBr) ν 3430.8, 3080.8, 2927.6, 1626.7, 1603.2, 1553.6, 1500.1, 1474.0, 1457.2, 1394.1, 1256.5, 1173.6, 1084.4, 1012.2, 878.7, 854.3, 767.2, 678.1, 580.4, 549.4, 527.6 cm^{-1}; HRMS (ESI-TOF): *m/z* calcd. for $C_{18}H_{18}N_3$, 276.1495; found, 276.1494.

4.1.11. 2,3-Diethyl-8H-10,11-dimethylpyridazino[2,3-a]pyrrolo[2,1-c]quinoxal-13-inium mesitylenesulfonate (*3j*)

Method D from **2e** (101.6 mg, 0.23 mmol). Yield: 78.7 mg (0.156 mmol, 68%); Orange solid; mp: 224–226 °C; ^{1}H NMR (300 MHz, CD_3OD): δ 8.71 (s, 1H, H-12), 8.70 (s, 1H, H-4), 8.8–8.6 (m, 1H, H-7), 8.24 (s, 1H, H-9), 8.06 (d, 1H, *J* = 4.1 Hz, H-5), 7.24 (dd, 1H, *J* = 4.1 Hz, *J* = 2.6 Hz, H-6), 6.80 (s, 2H, $H_{Ar\text{-}MSTS}$), 3.28 (q, 2H, *J* = 7.3 Hz, CH_2), 3.06 (q, 2H, *J* = 7.3 Hz, CH_2), 2.60 (s, 3H, CH_3), 2.58 (s, 6H, 2 $CH_{3\text{-}MSTS}$), 2.57 (s, 3H, CH_3), 2.20 (s, 3H, $CH_{3\text{-}MSTS}$), 1.59 (t, 3H, *J* = 7.3 Hz, CH_3), 1.52 (t, 3H, *J* = 7,3 Hz, CH_3) ppm; ^{13}C NMR (75 MHz, CD_3OD): δ 151.4, 144.4, 139.9, 138.9, 138.6, 138.2, 131.6 (2C), 127.1 (2C), 126.9, 126.4, 122.8, 121.4, 121.1, 119.1, 118.1, 117.8, 117.7, 116.0, 27.4, 25.8, 23.3 (2C), 20.8, 20.3, 20.1, 12.3, 11.1 ppm; IR (KBr) ν 3435.9, 3090.6, 2970.2, 2918.8, 2358.9, 2341.6, 1624.4, 1552.1, 1455.0, 1386.7, 1190.1, 1084.3, 1016.4, 879.8, 849.5, 765.7, 675.7 cm^{-1}; HRMS (ESI-TOF): *m/z* calcd. for $C_{20}H_{22}N_3$, 304.1808; found, 304.1820.

4.1.12. 7-Bromo-8H-10,11-dimethylpyridazino[2,3-a]pyrrolo[2,1-c]quinoxal-13-inium mesitylenesulfonate (*3k*)

Method B from **2f** (94.7 mg, 0.19 mmol) for 10 min. Yield: 59.4 mg (0.112 mmol, 59%); Green solid; mp: 205–206 °C; ^{1}H NMR (300 MHz, CD_3OD): δ 9.36 (s, 1H, H-12), 9.23 (dd, 1H, *J* = 4.4 Hz, *J* = 1.2 Hz, H-2), 9.09 (dd, *J* = 9.1 Hz, *J* = 1.2 Hz, H-4), 8.85 (s, 1H, H-9), 8,22 (q, 1H, *J* = 4.4 Hz, H-3), 8.15 (d, 1H, *J* = 4.4 Hz, H-6/H-5), 7.39 (d, 1H, *J* = 4.7 Hz, H-5/H-6), 6.84 (s, 2H, $H_{Ar\text{-}MSTS}$), 2.62 (s, 3H, CH_3), 2.59 (s, 6H, 2 $CH_{3\text{-}MSTS}$), 2.58 (s, 3H, CH_3), 2.23 (s, 3H, $CH_{3\text{-}MSTS}$) ppm; ^{13}C NMR (75 MHz, CD_3OD): δ 150.3, 143.7, 140.0, 139.6, 139.4, 138.8, 138.1, 132.8, 131.6 (2C), 131.3, 128.4 (2C), 127.3, 124.5, 124.3, 121.6, 118.4, 117.6, 109.6, 23.2 (2C), 20.8, 20.6, 19.9 ppm; IR (KBr) ν 3423.8, 3061.2, 2971.5, 2927.5, 1621.6, 1536.9, 1477.6; 1417.6, 1388.7, 1255.8, 1220.6, 1183.6, 1084.6, 1013.7, 902.8, 876.9, 848.3, 792.9, 677.6 cm^{-1}; HRMS (ESI-TOF): *m/z* calcd. for $C_{16}H_{13}^{79}BrN_3$ $[M]^+$, 326.0287; found, 326.0289.

4.1.13. 7-Bromo-8H-2,3,10,11-tetramethylpyridazino[2,3-a]pyrrolo[2,1-c]quinoxal-13-inium mesitylenesulfonate (*3l*)

Method A from **2f** (96.4 mg, 0.19 mmol) for 10 min. Yield: 96.1 mg (0.17 mmol, 91%); Greenish solid; mp: 211–213 °C; ^{1}H NMR (300 MHz, CD_3OD): δ 9.30 (s, 1H, H-12), 8.83 (s, 1H, H-9/H-4), 8.82 (s, 1H, H-4/H-9), 8.02 (d, 1H, *J* = 4.7 Hz, H-5), 7.30 (d, 1H, *J* = 4.4 Hz, H-6), 6.81 (s, 2H, $H_{Ar\text{-}MSTS}$), 2.86 (s, 3H, CH_3), 2.71 (s, 3H, CH_3), 2.59 (s, 3H, CH_3), 2.58 (s, 6H, $CH_{3\text{-}MSTS}$), 2.21 (s, 3H, $CH_{3\text{-}MSTS}$) ppm; ^{13}C NMR (75 MHz, CD_3OD): δ 161.5, 147.4, 142.8, 139.9, 139.2, 138.1, 138.0, 131.6 (2C), 128.5 (2C), 128.1, 126.9, 124.0, 123.7, 121.4, 118.3, 116.6, 108.3, 101.4, 23.2 (2C), 20.8, 20.6, 20.5, 19.9, 19.4 ppm; IR (KBr) ν 3413.9, 3072.9, 2918.5, 2360.0, 2314.6, 1626.0, 1594.8, 1552.7, 1478.3, 1393.4, 1262.3, 1187.6, 1083.4, 1013.0, 912.8, 884.5, 848.9, 802.1, 676 cm^{-1}; HRMS (ESI-TOF): *m/z* calcd. for $C_{18}H_{17}^{79}BrN_3$ $[M]^+$, 354.0600; found, 354.0603.

4.1.14. 8H-2,3-dimethyl-11-methoxypyridazino[2,3-a]pyrrolo[2,1-c]quinoxal-13-inium mesitylenesulfonate (*3m*)

Method A from **2g** (117.2 mg; 0.27 mmol) for 30 min. Yield: 49.9 mg (0.104 mmol, 38%); Dark-green solid; mp: 273–274 °C; ^{1}H NMR (200 MHz, CD_3OD): δ 8.87 (s, 1H, H-4), 8.66 (bs, 1H, H-7), 8.43 (d, 1H, *J* = 2.5 Hz, H-12), 8.38 (d, 1H, *J* = 9,3 Hz, H-9), 7.98 (d, 1H, *J* = 4.2 Hz, H-5), 7.58 (dd, 1H, *J* = 9,3 Hz, *J* = 2.5 Hz, H-10). 7,25 (t_{app},

1H, $J = 3.4$ Hz, H-6), 6.85 (s, 2H, $H_{Ar\text{-}MSTS}$), 4.06 (s, 3H, CH_3O), 2.87 (s, 3H, CH_3), 2.73 (s, 3H, CH_3). 2.62 (s, 6H, $CH_{3\text{-}MSTS}$), 2.23 (s, 3H, $CH_{3\text{-}MSTS}$) ppm; ^{13}C NMR (75 MHz, CD_3OD): δ 161.1, 160.2, 147.5, 140.8, 139.9, 139.5, 138.1, 131.6 (2C), 129.2; 128.9 (2C), 123.0, 122.9, 121.4, 121.3, 118.9, 118.1, 115.7, 103.9, 56.8, 23.3 (2C), 20.8, 20.5, 19.5 ppm; IR (KBr) ν 3468.5, 2930.4, 1623.4, 1555.6, 1535.5, 1508.8, 1458.7, 1396.6, 1318.0, 1257.0, 1085.9, 1016.1, 853.0, 842.7, 750.6, 677.1, 609.5, 579.6, 548.1 cm^{-1}; HRMS (ESI^+): *m/z* calcd. for $C_{17}H_{16}N_3O$, 278.1288; found, 278.1291.

4.1.15. 11-Trifluoromethyl-8H-2,3-dimethylpyridazino[2,3-a] pyrrolo[2,1-c]quinoxal-13-inium mesitylenesulfonate (**3n**)

Method B from **2h** (103.1 mg, 0.22 mmol) for 10 min. Yield: 54.4 mg (0.106 mmol, 48%); Black solid; mp: 288−290 °C; ^1H NMR (300 MHz, CD_3OD): δ 9.23 (s, 1H), 8.93 (s, 1H), 8.80 (dd, 1H, $J = 2.6$ Hz, $J = 1.3$ Hz), 8.63 (d, 1H, $J = 8.8$ Hz), 8.24 (d, 1H, $J = 8.8$ Hz), 8.09 (dd, 1H, J = 4,1 Hz, J = 1.3 Hz), 7.32 (dd, 1H, J = 4.1 Hz; $J = 2.9$ Hz), 6.77 (s, 2H), 2.89 (s, 3H), 2.75 (s, 3H), 2.55 (s, 6H), 2.19 (s, 3H) ppm; ^{13}C NMR (75 MHz, CD_3OD): δ 161.9, 149.1, 140.8, 140.5, 139.9, 138.1, 131.6 (2C), 129.6, 129.1 (2C), 124.4, 122.1, 119.1, 119.0, 117.6, 23.2 (2C), 20.8, 20.5, 19.3 ppm; IR (KBr): ν 3448.2, 3105.8, 2360.9, 1629.5, 1458.0, 1335.0, 1317.7, 1126.4, 1074.8, 1014.9, 832.3, 807.2, 677.3, 578.8, 549.0 cm^{-1}; HRMS (ESI^+): *m/z* calcd. for $C_{17}H_{13}F_3N_3$, 316.1056; found, 316.1051.

4.1.16. 10,11-Dichloro-8H-2,3-dimethylpyridazino[2,3-a]pyrrolo [2,1-c]quinoxal-13-inium mesitylenesulfonate (**3o**)

Method A from **2i** (132.2 mg, 0.28 mmol) y for 20 min. Yield: 51.6 mg (0.1 mmol, 35%); Black solid; mp: 289−290 °C; ^1H NMR (200 MHz, CD_3OD): δ 9.3 (s, 1H, H-12), 8.92 (s, 1H, H-9), 8.82 (s, 1H, H-4), 8.76 (d, 1H, J = 2,5 Hz, H-7), 8.06 (d, 1H, J = 4,2 Hz, H-5), 7.29 (t_{app}, 1H, $J = 3.6$ Hz, H-6), 6.82 (s, 2H, $H_{Ar\text{-}MSTS}$), 2.88 (s, 3H, CH_3), 2.74 (s, 3H, CH_3), 2.61 (s, 6H, $CH_{3\text{-}MSTS}$), 2.25 (s, 3H, $CH_{3\text{-}MSTS}$) ppm; ^{13}C NMR (75 MHz, CD_3OD): δ 149.3, 143.7, 140.7, 140.1, 140.0, 138.1, 137.9, 137.5, 136.2, 132.3, 131.6 (2C), 129.0, 128.3 (2C), 124.4, 123.0, 119.6, 118.9, 117.4, 23.2 (2C), 20.8, 20.4, 19.5 ppm; IR (KBr): ν 3422.3, 3080.6, 1603.1, 1499.3, 1372.1, 1288.6, 1188.2, 1084.7, 1015.4, 885.7, 848.6, 762.8, 677.7, 581.7 cm^{-1}; HRMS (ESI^+): *m/z* calcd. for $C_{16}H_{12}Cl_2N_3$, 316.0403; found, 316.0401.

4.2. Biological activity

4.2.1. Materials and reagents

All reagents for the *Li*TryR and "in cellulo" assays were obtained from Sigma-Aldrich (Saint Louis, MO, USA) except for TS_2, M199 and RPMI-1640 mediums, which were purchased from Bachem (Bubendorf, Switzerland), Gibco (Leiden, The Netherlands) and Lonza (Basel, Switzerland), respectively.

4.2.2. Leishmania cell lines and culture

L. infantum promastigotes (MCAN/ES/89/IPZ229/1/89) were grown in RPMI-1640 medium with L-glutamine (Lonza, Basel, Switzerland) supplemented with 10% heat-inactivated fetal calf serum (FCS), antibiotics, and 25 mM HEPES (pH 7.2) at 26 °C. *L. infantum* axenic amastigotes (MCAN/ES/89/IPZ229/1/89) were grown in M199 medium (Gibco, Leiden, The Netherlands) supplemented with 10% heat-inactivated FCS, 1 g/L β-alanine, 100 mg/L L-asparagine, 200 mg/L sucrose, 50 mg/L sodium pyruvate, 320 mg/L malic acid, 40 mg/L fumaric acid, 70 mg/L succinic acid, 200 mg/L α-ketoglutaric acid, 300 mg/L citric acid, 1.1 g/L sodium bicarbonate, 5 g/L MES, 0.4 mg/L hemin, and 10 mg/L gentamicine, pH 5.4, at 37 °C.

4.2.3. Axenization of L. infantum promastigotes

Axenization was performed by diluting 0.5 mL of a 7-day stationary phase culture of *L. infantum* promastigotes (approximately 2-3 x 10^7 parasites/mL) in 4.5 mL of amastigotes medium and incubating the culture at 37 °C for 3 days. Promastigote to amastigote differentiation was followed daily by phase-contrast microscopy in an Eclipse Ti inverted microscope (Nikon, Tokyo, Japan).

4.2.4. Leishmanicidal activity

L. infantum axenic amastigotes were treated during the logarithmic growth phase at a concentration of 10^6 parasites/mL at 37 °C for 24 h. EC_{50} was assessed by flow cytometry by the propidium iodide (PI) exclusion method. Briefly, after selection of the parasites population based on their forward scatter (FSC) and side scatter (SSC) values, live and dead parasite cells were identified by their different permeability to propidium iodide (PI). All the assays were performed in triplicate in three independent experiments. Data were analyzed using a nonlinear regression model with the GraFit 6 software (Erithacus, Horley, Surrey, UK).

4.2.5. THP-1 cell line and culture

THP-1 cells were grown in RPMI-1640 medium with L-glutamine (Lonza, Basel, Switzerland) supplemented with 10% heat inactivated FCS, antibiotics, 10 mM HEPES and 1 mM sodium pyruvate, pH 7.2, at 37 °C and 5% CO_2.

4.2.6. Cytotoxicity assays

Drug treatment of THP-1 cells was performed during the logarithmic growth phase at a concentration of 4×10^5 cells/mL at 37 °C and 5% CO_2 for 24 h. EC_{50} was evaluated by flow cytometry by PI exclusion method. All the assays were conducted in triplicate in three independent experiments. Data were analyzed using a nonlinear regression model with the GraFit 6 software (Erithacus, Horley, Surrey, UK).

4.2.7. In vitro infection of THP-1 derived macrophages with GFP-expressing L. infantum axenic amastigotes

THP-1 monocytes were seeded in a 24-well plate (Nunc, Roskilde, Denmark) at a concentration of 120,000 cells/mL (1 mL/well) in RPMI complete medium supplemented with phorbol 12-myristate 13-acetate (100 ng/mL). Differentiation of THP-1 monocytes to macrophages was achieved after 24 h at 37 °C and 5% CO_2. Following removal of the medium, THP-1 derived macrophages were infected with GFP-expressing axenic amastigotes at 1.2×10^6 parasites/mL in RPMI complete medium for 4 h (1 mL/well) at 37 °C and 5% CO_2. Extracellular amastigotes were subsequently removed, and THP-1 derived macrophages were washed three times with PBS. Treatments were performed in 1 mL of fresh RPMI complete medium during 48 h at 37 °C and 5% CO_2. Afterwards, treatments were removed by three PBS washes. Detachment of THP-1 derived macrophages was performed with TrypLE Express (Invitrogen, Leiden, The Netherlands) following a slightly modified version of the manufacturer's instructions (200 μL/well). Briefly, after a 30 min incubation at 37 °C and 5% CO_2, the cell detachment reaction was stopped by adding RPMI complete medium (1 mL/well). Then, detached THP-1 derived macrophages were gently resuspended, transferred to 1.5 mL-microtubes and centrifuged for 5 min at 1000×*g* and room temperature. The supernatants were discarded, and the cell pellets were gently resuspended in PBS containing 10 μg/mL PI (400 μL/well). THP-1 derived macrophages were acquired by a Beckman Coulter FC500 flow cytometer (Brea, CA, USA) and each sample (100 μL) was acquired for 20 s. After selection of the THP-1 derived macrophages population based on their FSC and SSC values, live and amastigote-infected macrophages were identified by their PI exclusion and the green fluorescence from the intracellular GFP-expressing amastigotes, respectively. All

the assays were performed in three independent experiments. Data were analyzed using a nonlinear regression model with the GraFit 6 software (Erithacus, Horley, Surrey, UK).

4.2.8. LiTryR purification

Recombinant *Leishmania infantum* TryR (*Li*TryR) was purified from *Escherichia coli* as previously described (Toro et al., 2013). Briefly, a *pRSETA-HIS-LiTryR* construct was transformed into BL21 (DE3) Rossetta *E. coli* strain. An overnight *E. coli* culture grown at 37 °C in LB medium with suitable antibiotics and vigorous shaking was diluted (1:100) in the same medium and allowed to grow in the same conditions until the OD_{600} was 0.5. At that point, *Li*TryR expression was induced by addition of 1 mM isopropyl-beta-D-1-thiogalactopyranoside (IPTG) during 16 h at 26 °C. The cell culture was centrifuged for 5 min at 9000×*g* and 4 °C and the wet pellet resuspended in a lysis buffer containing 50 mM Tris pH 7, 300 mM NaCl, 25 mM imidazole, 1 mg/mL lysozyme and a protease inhibitor cocktail. After a 30 min incubation on ice, the lysate was sonicated on ice (50% pulses, potency 7) for 30 min using a Sonifier Cell Disruptor B15 (Branson, Danbury, CT, USA) and centrifuged during 1 h at 50,000×*g* and 4 °C. The supernatant was sonicated again as previously described for 10 min and continuously loaded onto a HisTrap column (GE Healthcare, Chicago, IL, USA) during 16 h at 4 °C using a peristaltic pump P-1 (GE Healthcare, Chicago, IL, USA). The HisTrap column was subsequently connected to an ÄKTApurifier UPC 10 (GE Healthcare, Chicago, IL, USA) and extensively washed using a 10% gradient between buffers A (50 mM Tris pH 7 and 300 mM NaCl) and B (50 mM Tris pH 7, 300 mM NaCl and 500 mM imidazole). *Li*TryR was eluted using a 40% gradient between buffer A and B. Fractions containing recombinant *Li*TryR were pooled and loaded onto a HiPrep™ 26/10 Desalting column (GE Healthcare, Chicago, IL, USA) to remove the imidazole. Finally, *Li*TryR was concentrated to 2 mg/mL using an Amicon® Ultra-15 50K (Merck Millipore, Burlington, MA, USA) and an equal volume of glycerol was added before its storage at −20 °C.

4.2.9. LiTryR oxidoreductase activity

*Li*TryR oxidoreductase activity was measured spectrophotometrically using a modified version of the standard DTNB-coupled assay described by Hamilton et al. (2003). Briefly, reactions (250 μL) were performed at 26 °C in HEPES buffer (pH 7.5, 40 mM) containing EDTA (1 mM), NADPH (150 μM), $NADP^+$ (30 μM), DTNB (25 μM), TS_2 (1 μM), glycerol (0.02%), DMSO (1.7%) and recombinant *Li*TryR (7 nM). *Li*TryR oxidoreductase activity was monitored at 26 °C by the increase in absorbance at 412 nm in an EnSpire Multimode Plate Reader (PerkinElmer, Waltham, MA, USA). All assays were performed in three independent experiments. Data were analyzed using a nonlinear regression model with the GraFit 6 software (Erithacus, Horley, Surrey, UK).

4.2.10. Determination of **3f** inhibition constant with NADPH as fixed substrate

The **3f** inhibition constant (K_i) with NADPH as fixed substrate was calculated following a slightly modified version of the standard DTNB-coupled assay developed by Hamilton et al. (2003). TS_2 was serially diluted in a buffer containing 40 mM HEPES (pH 7.5) and 1 mM EDTA to produce a 5-point range from 1666.6 μM to 104.2 μM. The different TS_2 solutions were added (15 μL) to a 96-well microplate. 3f was serially diluted in DMSO to produce a 5-point range from 2000 μM to 125 μM. The different aliquots of **3f** and the equivalent amount of the vehicle (DMSO) were added to a pre-assay mixture yielding different mixtures containing 40 mM HEPES (pH 7.5), 1 mM EDTA, 416.7 μM NADPH, 208.3 μM DTNB, 1.5% DMSO and, in certain cases, different concentrations of **3f** ranging from 27.8 μM to 1.7 μM. These mixtures (180 μL) were subsequently added to the appropriate wells previously filled with different TS_2 solutions. The assay was initiated by addition of 55 μL of a buffer containing 40 mM HEPES (pH 7.5), 1 mM EDTA, 272.7 μM $NADP^+$, 0.01% glycerol and 3.2 nM recombinant *Li*TryR using an automated dispensing system (PerkinElmer, Waltham, MA, USA). The order of addition was essential to avoid enzyme preincubation with the inhibitor or the substrates. The final assay mixtures contained 250 μL of 40 mM HEPES buffer (pH 7.5) 1 mM EDTA, 300 μM NADPH, 60 μM $NADP^+$, 150 μM, 100–6.2 μM TS_2, 1% DMSO, 0.002% glycerol and 0.7 nM recombinant *Li*TryR. Oxidoreductase activity of *Li*TryR was monitored at 26 °C by the increase in absorbance at 412 nm in an EnSpire Multimode Plate Reader (PerkinElmer, Waltham, MA, USA).

4.2.11. Determination of **3f** inhibition constant with TS_2 as fixed substrate

The K_i for **3f** with TS_2 as fixed substrate was calculated following a slightly modified version of the protocol described above. NADPH was serially diluted in a buffer containing 40 mM HEPES (pH 7.5) and 1 mM EDTA to produce a 7-point range from 5000 μM to 78.1 μM. The different NADPH solutions were added (15 μL) to a 96-well microplate. 3f was serially diluted in DMSO to produce a 3-point range from 250 μM to 62.5 μM. The different aliquots of **3f** and the equivalent amount of the vehicle (DMSO) were added to a pre-assay mixture yielding different mixtures containing 40 mM HEPES (pH 7.5), 1 mM EDTA, 138.9 μM TS_2, 208.3 μM DTNB, 1.5% DMSO and, in certain cases, different concentrations of **3f** ranging from 3.5 μM to 0.9 μM. These mixtures (180 μL) were subsequently added to the appropriate wells previously filled with different NADPH solutions. The assay was initiated by addition of 55 μL of a buffer containing 40 mM HEPES (pH 7.5), 1 mM EDTA, 272.7 μM $NADP^+$, 0.01% glycerol and 3.2 nM recombinant *Li*TryR using an automated dispensing system (PerkinElmer, Waltham, MA, USA). The final assay mixture contained 250 μL of 40 mM HEPES buffer (pH 7.5) 1 mM EDTA, 75–4.7 μM NADPH, 60 μM $NADP^+$, 150 μM, 100 μM TS_2, 1% DMSO, 0.002% glycerol and 0.7 nM recombinant *Li*TryR.

4.2.12. LiTryR-mediated cytochrome c reduction

The ability of **3f** to induce *Li*TryR-mediated cytochrome *c* reduction was measured spectrophotometrically using a modified version of the protocol previously described by Blumenstiel et al. [24]. Briefly, reactions (250 μL/well) were performed at 26 °C in potassium phosphate buffer (50 mM, pH 7.8) containing EDTA (1 mM), NADPH (150 μM), cytochrome *c* (40 μM), glycerol (2.8%), DMSO (1%), catalase from bovine liver (0.8 μM) and recombinant *Li*TryR (1 μM). Reactions were started by addition of NADPH (50 μL/well). In order to distinguish between the superoxide-mediated and direct reduction of cytochrome *c*, the oxidase reactions were followed in the absence and in the presence of 4 μM of *L. infantum* superoxide dismutase A. Menadione was used as positive control given its proven ability to induce the oxidase activity of *T. cruzi* TryR [18]. *Li*TryR-mediated cytochrome *c* reduction was monitored at 26 °C by the increase in absorbance at 550 nm in an EnSpire Multimode Plate Reader (PerkinElmer, Waltham, MA, USA). All assays were performed in three independent experiments.

4.2.13. Data analysis

GraFit 6.0 software (Erithacus, Horley, SRY, UK) was used to perform linear and nonlinear regressions. All experiments were performed in triplicate to ensure the reliability of single values.

The initial reaction rates of the progress curves at different **3f** and substrate concentrations were fitted to the linear rate equations that describe the reversible modes of inhibitor interactions with enzymes. Equations (1)–(3) are the velocity equations for

competitive, noncompetitive and uncompetitive inhibitors, respectively:

$$v = \frac{V_{max}[S]}{[S] + K_m\left(1 + \frac{[I]}{K_i}\right)} \quad (1)$$

$$v = \frac{V_{max}[S]}{[S]\left(1 + \frac{[I]}{\alpha K_i}\right) + K_m\left(1 + \frac{[I]}{K_i}\right)} \quad (2)$$

$$v = \frac{V_{max}[S]}{[S]\left(1 + \frac{[I]}{\alpha K_i}\right) + K_m} \quad (3)$$

The initial reaction rates of the progress curves at different **3f** and substrate concentrations were fitted to the nonlinear rate Equation (4) for inhibitors whose apparent values of $1/V_{max}$ or K_m/V_{max} display a nonlinear dependence on their concentration [15]:

$$v = \frac{V_{max}[S]}{K_m\left(\frac{1+\frac{[I]}{K_i}}{1+\frac{\beta[I]}{\alpha K_i}}\right) + [S]\left(\frac{1+\frac{[I]}{\alpha K_i}}{1+\frac{\beta[I]}{\alpha K_i}}\right)} \quad (4)$$

Dependency of the apparent values of K_m/V_{max} (slope) or $1/V_{max}$ (intercept) functions on inhibitor concentration was analyzed graphically using the following the equations [15]:

$$\text{Slope} = \frac{\alpha K_m}{V_{max}}\left(\frac{K_i + [I]}{\alpha K_i + \beta[I]}\right) \quad (5)$$

$$\text{Intercept} = \frac{1}{V_{max}}\left(\frac{\alpha K_i + [I]}{\alpha K_i + \beta[I]}\right) \quad (6)$$

4.3. Computational chemistry

Ab initio geometry optimizations and molecular orbital calculations for menadione and **3f** were achieved using a 6-31G* basis set and the density functional B3LYP method, as implemented in program Gaussian 09 (Revision D.01) [25]. Water effects were taken into account by means of the IEF-SCRF continuum solvent method [26]. Molecular orbitals were visualized with the aid of program Gabedit 2.5.0 [27].

Declaration of competing interest

The authors declare the following competing financial interest(s): P. S.-A., J. J. V., R. A., and A. J.-R. are coinventors on a patent application filled by the University of Alcalá describing the use of compounds 3 for the treatment of *Leishmania* infections (WO 2015004304).

Acknowledgements

This research was funded by the Spanish MICINN (Projects PID2019-104070RB-C22 and PCTQ2017-85263-R), the Comunidad de Madrid (Project PLATESA2-CM ref S-2018/BAA-4370 and NOVELREN, B2017/BMD-3751) and the Instituto de Salud Carlos III (FEDER funds, RETIC REDINREN RD16/0009/0015). The University of Alcalá and the Spanish Ministry for Culture and Education are gratefully acknowledged for the predoctoral fellowship (FPU16/01647) to J. G.-M. The University of Alcalá is also gratefully acknowledged for the FPU grants to P. S. A. and J. C. G.-S. and the postdoctoral fellowship to H. d. L.

Appendix A. Supplementary data

Supplementary data to this article can be found online at https://doi.org/10.1016/j.ejmech.2021.113915.

References

[1] P.D. Ready, Epidemiology of visceral leishmaniasis, Clin. Epidemiol. 6 (2014) 147–154, https://doi.org/10.2147/CLEP.S44267.
[2] F. Alves, G. Bilbe, S. Blesson, V. Goyal, S. Monnerat, C. Mowbray, G. Muthoni Ouattara, B. Pecoul, S. Rijal, J. Rode, et al., Recent development of visceral leishmaniasis treatments: successes, pitfalls, and perspectives, Clin. Microbiol. Rev. 31 (2018), https://doi.org/10.1128/CMR.00048-18.
[3] A. Ponte-Sucre, F. Gamarro, J.C. Dujardin, M.P. Barrett, R. Lopez-Velez, R. Garcia-Hernandez, A.W. Pountain, R. Mwenechanya, B. Papadopoulou, Drug resistance and treatment failure in leishmaniasis: a 21st century challenge, PLoS Neglected Trop. Dis. 11 (2017), e0006052, https://doi.org/10.1371/journal.pntd.0006052.
[4] E. Morelli, S. Gemma, R. Budriesi, G. Campiani, E. Novellino, C. Fattorusso, B. Catalanotti, S.S. Coccone, S. Ros, G. Borrelli, et al., Specific targeting of peripheral serotonin 5-HT3 receptors. Synthesis, biological investigation, and Structure–Activity relationships, J. Med. Chem. 52 (2009) 3548–3562, https://doi.org/10.1021/jm900018b.
[5] V. Desplat, S. Moreau, A. Gay, S.B. Fabre, D. Thiolat, S. Massip, G. Macky, F. Godde, D. Mossalayi, C. Jarry, et al., Synthesis and evaluation of the antiproliferative activity of novel pyrrolo[1,2-a]quinoxaline derivatives, potential inhibitors of Akt kinase. Part II, J. Enzym. Inhib. Med. Chem. 25 (2010) 204–215, https://doi.org/10.3109/14756360903169881.
[6] J. Garcia-Marin, M. Griera, P. Sanchez-Alonso, B. Di Geronimo, F. Mendicuti, M. Rodriguez-Puyol, R. Alajarin, B. de Pascual-Teresa, J.J. Vaquero, D. Rodriguez-Puyol, Pyrrolo[1,2-a]quinoxalines: insulin mimetics that exhibit potent and selective inhibition against protein tyrosine phosphatase 1B, ChemMedChem 15 (2020) 1788–1801, https://doi.org/10.1002/cmdc.202000446.
[7] H. Xu, L.-l. Fan, Synthesis and antifungal activities of novel 5,6-dihydro-indolo [1,2-a]quinoxaline derivatives, Eur. J. Med. Chem. 46 (2011) 1919–1925, https://doi.org/10.1016/j.ejmech.2011.02.035.
[8] J. Guillon, I. Forfar, M. Mamani-Matsuda, V. Desplat, M. Saliège, D. Thiolat, S. Massip, A. Tabourier, J.-M. Léger, B. Dufaure, et al., Synthesis, analytical behaviour and biological evaluation of new 4-substituted pyrrolo[1,2-a]quinoxalines as antileishmanial agents, Bioorg. Med. Chem. 15 (2007) 194–210, https://doi.org/10.1016/j.bmc.2006.09.068.
[9] J. Guillon, E. Mouray, S. Moreau, C. Mullie, I. Forfar, V. Desplat, S. Belisle-Fabre, N. Pinaud, F. Ravanello, A. Le-Naour, et al., New ferrocenic pyrrolo[1,2-a]quinoxaline derivatives: synthesis, and in vitro antimalarial activity–Part II, Eur. J. Med. Chem. 46 (2011) 2310–2326, https://doi.org/10.1016/j.ejmech.2011.03.014.
[10] A. Jonet, J. Guillon, C. Mullie, A. Cohen, G. Bentzinger, J. Schneider, N. Taudon, S. Hutter, N. Azas, S. Moreau, et al., Synthesis and antimalarial activity of new enantiopure aminoalcoholpyrrolo[1,2-a]quinoxalines, Med. Chem. 14 (2018) 293–303, https://doi.org/10.2174/1573406413666170726123938.
[11] L. Ronga, M. Del Favero, A. Cohen, C. Soum, P. Le Pape, S. Savrimoutou, N. Pinaud, C. Mullie, S. Daulouede, P. Vincendeau, et al., Design, synthesis and biological evaluation of novel 4-alkapolyenylpyrrolo[1,2-a]quinoxalines as antileishmanial agents–part III, Eur. J. Med. Chem. 81 (2014) 378–393, https://doi.org/10.1016/j.ejmech.2014.05.037.
[12] L. van Heerden, T.T. Cloete, J.W. Breytenbach, C. de Kock, P.J. Smith, J.C. Breytenbach, D.D. N'Da, Synthesis and in vitro antimalarial activity of a series of bisquinoline and bispyrrolo[1,2a]quinoxaline compounds, Eur. J. Med. Chem. 55 (2012) 335–345, https://doi.org/10.1016/j.ejmech.2012.07.037.
[13] J. García-Marín, M. Griera, R. Alajarín, M. Rodríguez-Puyol, D. Rodríguez-Puyol, J.J. Vaquero, A computer-driven scaffold-hopping approach generating new PTP1B inhibitors from the pyrrolo[1,2-a]quinoxaline core, *ChemMedChem*, **n/a** (2021), https://doi.org/10.1002/cmdc.202100338.
[14] P. Sánchez-Alonso, M. Griera, J. García-Marín, M. Rodríguez-Puyol, R. Alajarín, J.J. Vaquero, D. Rodríguez-Puyol, Pyrrolo[1,2-a]quinoxal-5-inium salts and 4,5-dihydropyrrolo[1,2-a]quinoxalines: synthesis, activity and computational docking for protein tyrosine phosphatase 1B, Bioorg. Med. Chem. 44 (2021) 116295, https://doi.org/10.1016/j.bmc.2021.116295.
[15] A. Molina, J.J. Vaquero, J.L. Garcia-Navio, J. Alvarez-Builla, B. de Pascual-Teresa, F. Gago, M.M. Rodrigo, Novel DNA intercalators based on the pyridazino[1',6':1,2]pyrido[4,3-b]indol-5-inium system, J. Org. Chem. 64 (1999) 3907–3915, https://doi.org/10.1021/jo982216d.
[16] J. Pastor, J.G. Siro, J.L. García-Navío, J.J. Vaquero, J. Alvarez-Builla, F. Gago, B. de Pascual-Teresa, M. Pastor, M.M. Rodrigo, Azino-fused benzimidazolium salts as DNA intercalating agents. 2, J. Org. Chem. 62 (1997) 5476–5483, https://

doi.org/10.1021/jo962055i.
[17] G. De Muylder, K.K. Ang, S. Chen, M.R. Arkin, J.C. Engel, J.H. McKerrow, A screen against *Leishmania* intracellular amastigotes: comparison to a promastigote screen and identification of a host cell-specific hit, PLoS Neglected Trop. Dis. 5 (2011), e1253, https://doi.org/10.1371/journal.pntd.0001253.
[18] M. De Rycker, I. Hallyburton, J. Thomas, L. Campbell, S. Wyllie, D. Joshi, S. Cameron, I.H. Gilbert, P.G. Wyatt, J.A. Frearson, et al., Comparison of a high-throughput high-content intracellular *Leishmania donovani* assay with an axenic amastigote assay, Antimicrob. Agents Chemother. 57 (2013) 2913–2922, https://doi.org/10.1128/AAC.02398-12.
[19] V. Leskovac (Ed.), Comprehensive Enzyme Kinetics, Springer, Boston MA, 2003.
[20] N. Cenas, D. Bironaite, E. Dickancaite, Z. Anusevicius, J. Sarlauskas, J.S. Blanchard, Chinifur, a selective inhibitor and "subversive substrate" for *Trypanosoma congolense* trypanothione reductase, Biochem. Biophys. Res. Commun. 204 (1994) 224–229, https://doi.org/10.1006/bbrc.1994.2448. S0006-291X(84)72448-X.
[21] D. Spinks, E.J. Shanks, L.A. Cleghorn, S. McElroy, D. Jones, D. James, A.H. Fairlamb, J.A. Frearson, P.G. Wyatt, I.H. Gilbert, Investigation of trypanothione reductase as a drug target in *Trypanosoma brucei*, ChemMedChem 4 (2009) 2060–2069, https://doi.org/10.1002/cmdc.200900262.
[22] C. Morin, T. Besset, J.-C. Moutet, M. Fayolle, M. Brückner, D. Limosin, K. Becker, E. Davioud-Charvet, The aza-analogues of 1,4-naphthoquinones are potent substrates and inhibitors of plasmodial thioredoxin and glutathione reductases and of human erythrocyte glutathione reductase, Org. Biomol. Chem. 6 (2008) 2731–2742, https://doi.org/10.1039/B802649C.
[23] M. Elhabiri, P. Sidorov, E. Cesar-Rodo, G. Marcou, D.A. Lanfranchi, E. Davioud-Charvet, D. Horvath, A. Varnek, Electrochemical properties of substituted 2-methyl-1,4-naphthoquinones: redox behavior predictions, Chem. Eur J. 21 (2015) 3415–3424, https://doi.org/10.1002/chem.201403703.
[24] K. Blumenstiel, R. Schöneck, V. Yardley, S.L. Croft, R.L. Krauth-Siegel, Nitrofuran drugs as common subversive substrates of *Trypanosoma cruzi* lipoamide dehydrogenase and trypanothione reductase, Biochem. Pharmacol. 58 (1999) 1791–1799, https://doi.org/10.1016/S0006-2952(99)00264-6.
[25] M.J. Frisch, G.W. Trucks, H.B. Schlegel, G.E. Scuseria, M.A. Robb, J.R. Cheeseman, G. Scalmani, V. Barone, B. Mennucci, G.A. Petersson, et al., Gausian, Inc., Wallingford, CT, 2016.
[26] G. Scalmani, M.J. Frisch, Continuous surface charge polarizable continuum models of solvation. I. General formalism, J. Chem. Phys. 132 (2010) 114110, https://doi.org/10.1063/1.3359469.
[27] A.-R. Allouche, Gabedit—a graphical user interface for computational chemistry softwares, J. Comput. Chem. 32 (2011) 174–182, https://doi.org/10.1002/jcc.21600.